AGU PUBLICATIONS

JGR

Journal of Geophysical Research: Oceans

RESEARCH ARTICLE

10.1002/2017JC012865

Special Section:

Atmosphere-ice-ocean-ecosystem Processes in a Thinner Arctic Sea Ice Regime: The Norwegian Young Sea ICE Cruise 2015 (N-ICE2015)

Thin Sea Ice, Thick Snow, and Widespread Negative Freeboard Observed During N-ICE2015 North of Svalbard

Anja Rösel[1], Polona Itkin[1], Jennifer King[1], Dmitry Divine[1], Caixin Wang[1], Mats A. Granskog[1], Thomas Krumpen[2], and Sebastian Gerland[1]

[1]Norwegian Polar Institute, Tromsø, Norway, [2]Alfred Wegener Institute, Bremerhaven, Germany

Key Points:

- During N-ICE2015 the snow-to-ice thickness ratio was exceptionally high due to thick snow on thin ice
- Modal sea-ice thickness was below historical observations in the area north of Svalbard confirms the general trend of continued thinning
- Thick snow limited ice growth in winter, resulting in flooding and widespread negative freeboard

Supporting Information:

- Supporting Information S1

Correspondence to:

A. Rösel,

anja.rosel@npolar.no

Citation:

Rösel, A., Itkin, P., King, J., Divine, D., Wang, C., Granskog, M. A., . . . Gerland, S. (2018). Thin sea ice, thick snow and widespread negative freeboard observed during N-ICE2015 north of Svalbard. *Journal of Geophysical Research: Oceans*, *123*. https://doi.org/10.1002/2017JC012865

Received 8 MAR 2017

Accepted 10 JAN 2018

Accepted article online 1 FEB 2018

Abstract In recent years, sea-ice conditions in the Arctic Ocean changed substantially toward a younger and thinner sea-ice cover. To capture the scope of these changes and identify the differences between individual regions, in situ observations from expeditions are a valuable data source. We present a continuous time series of in situ measurements from the N-ICE2015 expedition from January to June 2015 in the Arctic Basin north of Svalbard, comprising snow buoy and ice mass balance buoy data and local and regional data gained from electromagnetic induction (EM) surveys and snow probe measurements from four distinct drifts. The observed mean snow depth of 0.53 m for April to early June is 73% above the average value of 0.30 m from historical and recent observations in this region, covering the years 1955–2017. The modal total ice and snow thicknesses, of 1.6 and 1.7 m measured with ground-based EM and airborne EM measurements in April, May, and June 2015, respectively, lie below the values ranging from 1.8 to 2.7 m, reported in historical observations from the same region and time of year. The thick snow cover slows thermodynamic growth of the underlying sea ice. In combination with a thin sea-ice cover this leads to an imbalance between snow and ice thickness, which causes widespread negative freeboard with subsequent flooding and a potential for snow-ice formation. With certainty, 29% of randomly located drill holes on level ice had negative freeboard.

1. Introduction

Sea-ice conditions in the Arctic have undergone substantial change in recent years, transitioning from a multiyear ice dominated, to a younger and thinner ice cover (e.g., Hansen et al., 2013; Kwok & Rothrock, 2009; Maslanik et al., 2011). A decline in sea-ice extent is well documented, since 1979, through the use of satellite observations (Comiso et al., 2008; Meier et al., 2014) and in modeling studies (e.g., Hunke et al., 2010; Stroeve et al., 2007). A corresponding decline in sea-ice thickness has been shown from direct observations (e.g., Haas et al., 2011; Lindsay & Schweiger, 2015), from satellite altimetry data (e.g., Kwok & Cunningham, 2015; Laxon et al., 2013), from radiometric data (Kaleschke et al., 2015), and also from altimetry data in combination with radiometric data (Ricker et al., 2017).

Field studies and direct observations allow the investigation of the composition of ice types (Hansen et al., 2014), the amount and structure of the snow cover (Haapala et al., 2013; Webster et al., 2014), and the seasonal changes in ice and snow thickness (Perovich et al., 2014; Wang et al., 2016). Regional (e.g., Hansen et al., 2013; King et al., 2017; Renner et al., 2013, 2014) and local studies (Gerland et al., 2008) in the European sector of the Arctic Ocean have shown a thinning of sea-ice coherent with that documented on a pan-Arctic scale.

Regional Arctic sea-ice studies in early winter are few; i.e., Nansen's Fram drift at the end of the 19th century, the Surface Heat Budget of the Arctic Ocean study (SHEBA), from October 1997 to October 1998 in the Beaufort Sea (e.g., Perovich, 2003), and the transpolar drift of the schooner *Tara* in 2007–2008 (Gascard et al., 2008; Haas et al., 2011). Another valuable data sources are observations made at Soviet drifting stations and aircraft landings on Arctic sea ice, compiled by Radionov et al. (1997) and Romanov (1996) and published by Warren et al. (1999) (hereafter W99). In the past decade, intensive measurements of snow and ice thickness mainly over the western and central Arctic are performed by NASA's Operation Ice Bridge's aircraft overflights (e.g., Richter-Menge & Farrell, 2013).

The Norwegian young sea ICE expedition (N-ICE2015), led by the Norwegian Polar Institute in the region north of Svalbard, from January to June 2015 therefore represents a unique opportunity to study the conditions found for a changing Arctic sea-ice regime. The multidisciplinary expedition documented the

conditions in a younger and thinner ice pack, with a special focus on the transition from polar night to spring (Granskog et al., 2016).

Snow is a key component of the ocean-ice-atmosphere system. Sea-ice and snow thickness control heat fluxes and radiative transfer that are key parameters for describing and quantifying ice-ocean-atmosphere interactions. Additionally, snow has a large impact on sea-ice thermodynamics: In winter, the low density snow pack is an insulator from a cold atmosphere and at the same time it prevents a warming of the atmosphere by a comparably warm Arctic Ocean (Gallet et al., 2017; Sturm, 2002). These characteristics control the wintertime growth rate of the underlying sea ice (Perovich, 2003). A thicker snow pack on relatively thin ice can become a positive contribution to the sea-ice mass balance through snow-ice formation (Granskog et al., 2017; Haas et al., 2001; Provost et al., 2017).

The most widely used snow depth data remains the pan-Arctic snow climatology from observations made during Soviet drifting stations on multiyear Arctic sea ice from W99, while other snow on sea-ice data products from airborne data (e.g., Kurtz et al., 2013; Newman et al., 2014) and remote sensing data (Maaß et al., 2013) are still under development.

Bintanja and Selten (2014), Park et al. (2015) Woods and Caballero (2016), Graham et al. (2017a), and Rinke et al. (2017) suggest that there is strong evidence of a change of the Arctic climate regime, especially for the Atlantic sector toward a higher storm frequency and more precipitation events. An increase in frequency and duration of winter warming events in the North Pole region, from the Atlantic sector is shown by Graham et al. (2017b). Assuming the precipitation falls as snow and with thinning ice this may cause the sea-ice regime in this region to shift toward conditions more commonly associated with Antarctic sea ice; thin ice with a deep snow cover, which promotes negative freeboard.

In the context of sea-ice and snow observations as well as heat fluxes during N-ICE2015, some relevant studies have been already published: Merkouriadi et al. (2017a) and Gallet et al. (2017) describe snow pack properties and it's transition from winter to summer. They describe a unique snow stratigraphy with a distinct depth hoar layer in the bottom that impacts the thermal conductivity of the snow. Granskog et al. (2017) and Provost et al. (2017) report a significant snow-ice formation from ice core analyses and buoy observations, caused by an increased snow-to-ice thickness ratio. Provost et al. (2017) also calculates the heat fluxes between ocean, ice, and atmosphere. Peterson et al. (2017) and Meyer et al. (2017a) observed the heat fluxes from the ocean to the ice. They find that storms significantly control heat fluxes and particularly above Atlantic Water they are inducing rapid basal melt events. With reference to a thinner, and therefore more fragile sea-ice cover Itkin et al. (2017) report strong deformation rates during the expedition and state that storm events can irreversibly damage the sea-ice cover.

This paper presents a comprehensive compilation and analysis of sea-ice and snow mass balance observations, consisting of in situ measurements of sea-ice, snow thickness, and freeboard collected in the vicinity of the vessel, *RV Lance*, and regional scale airborne survey data.

The paper is structured as follows: In Section 2 and 3, the expedition and the methods are described, followed by the presentation of the results (section 4). Thereafter, in section 5, we discuss the results and demonstrate the important role of snow in the sea-ice mass balance in a changing Arctic sea-ice regime. When set in the context of historical observations in the same region (section 5.2), the data indicate a decrease in sea-ice thickness, and a deeper than expected snow pack. Finally, we summarize the findings in section 6.

2. The N-ICE2015 Expedition

The N-ICE2015 drift experiment started north of Svalbard at 83°15′N, 21°32′E on 15 January 2015. The Norwegian research vessel *RV Lance* was used as a drifting base and logistic platform, moored to and drifting with a sea-ice floe. Once the ship drifted out of the consolidated ice pack or the ice floe broke up it was relocated toward the original starting area and a new drift started. As a result, the ship drifted four times within a region that extended between 80°N–83°N and 3°E–28°E (Granskog et al., 2016), which we refer hereafter as the area north of Svalbard. On each of the drifts an ice camp was established, these are referred to hereafter as *Floe 1*, *Floe 2*, *Floe 3*, and *Floe 4* (Figure 1). The ice floes were selected based on the following criteria: location within helicopter range from Svalbard for search and rescue operations, accessibility and mooring possibilities for the vessel, sufficient floe diameter and thickness to support the science program, proximity to level first-year ice

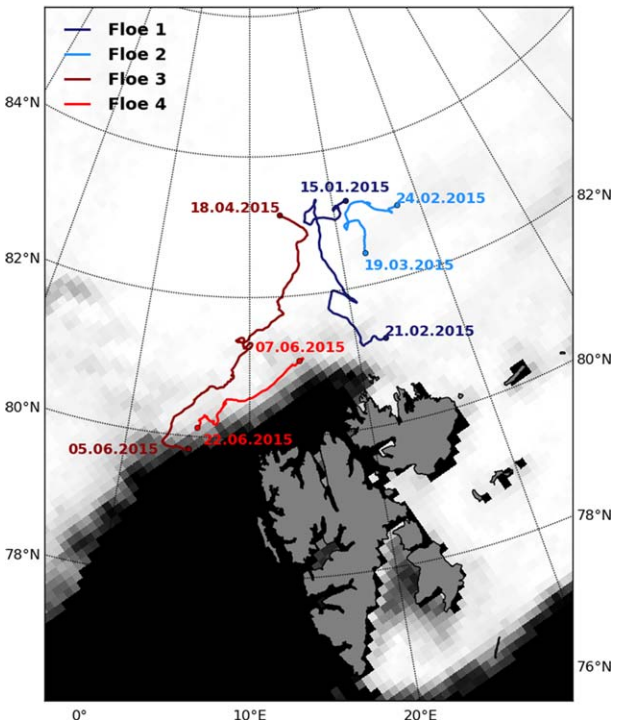

Figure 1. Trajectories of the four N-ICE2015 drifts in the area north of Svalbard. The background is sea-ice concentration (black is 0%; white is 100% sea-ice concentration) from 15 May 2015 based on SSM/I data, calculated with ASI algorithm, provided by ICDC, University Hamburg.

(FYI), and representativeness of the surrounding sea ice. The layout of the ice camps varied depending on the surface topography and dimensions of each floe and covered a range of different ice types. Schematics for the survey setups, ice type composition, and the snow and ice thickness sampling sites for each drift station are presented in Figure 2.

Calculated back trajectories for the four drift stations, based on drift-vectors extracted from passive microwave sea-ice drift product (Girard-Ardhuin & Ezraty, 2012) show that the oldest sea ice in the investigated area originates from the northern Laptev Sea, and initially formed in September 2013 (Itkin et al., 2017). In addition to this second-year ice (SYI), the region contained both FYI floes and young ice (YI) produced in refrozen leads during the time period of the drift.

3. Data and Methods

The ground-based surveys during N-ICE2015 consists of stationary time series and measurements with spatial coverage. In the first category, autonomous buoys provide time series of snow accumulation and snow depth and ice thickness. In the second category, snow and ice thickness surveys were performed along transects with a snow probe and electromagnetic soundings. We describe first the methods that generate a stationary time series (sections 3.1 and 3.2) and then the surveys with spatial coverage (section 3.3).

3.1. Autonomous Buoys

Buoys are used as autonomous platforms that record a variety of data and transmit these regularly via the Iridium satellite network. For this paper, we analyzed the snow and sea-ice mass balance data recorded by three types of buoys: snow buoys, thermistor ice mass balance buoys (IMB), and seasonal IMBs.

Snow buoys (developed by MetOcean Data Systems, Dartmouth, Canada) measure the distance to the snow surface with four sonic sensors. The snow buoys cannot provide any information on the internal

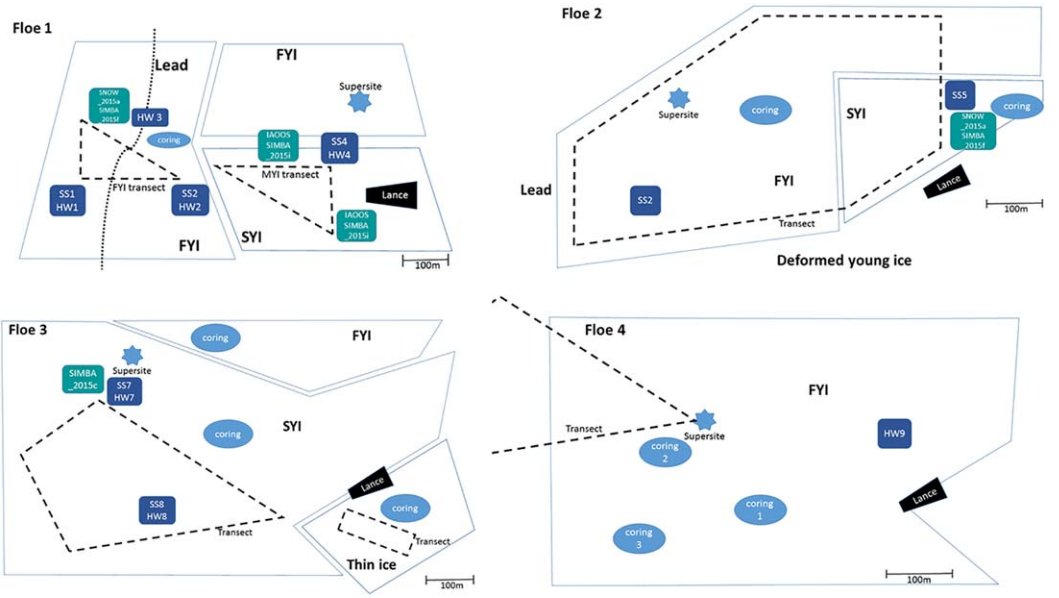

Figure 2. Sketches of the four N-ICE2015 ice stations (*Floes 1–4*) with their sea-ice mass balance related installations and tracks.

structure of the snow or detect subsurface changes, e.g., snow-ice or superimposed ice formation. At deployment, the initial snow depth was measured and afterward used to calibrate the values measured by the buoy. Thermistor IMBs are designed to measure temperatures along a cable deployed through a profile of air, snow, ice, and surface ocean. During N-ICE2015 two types of thermistor IMBs were deployed: SAMS (Scottish Association for Marine Science) Ice Mass Balance for the Arctic (SIMBA) buoys, produced by SAMS Research Services Ltd. (SRSL) (Jackson et al., 2013) and IMB-Bs, produced by British Antarctic Survey (Cambridge, UK) and Bruncin (Zagreb, Croatia). Both are equipped with a 5 m long thermistor chain cable hanging from a tripod through air, snow, and a 2 in. drill hole through the sea ice into the ocean.

The buoy measures temperature with 20 mm vertical resolution at approximately 0.1°C accuracy. They also feature a heating mode that provides a proxy for thermal resistivity (the proxy is calculated from temperature differences after a heating cycle) which can be used to discriminate between different media, especially between air, snow, and ice. The interfaces were defined using the method described in Provost et al. (2017) and an example is shown in Figure 3.

The seasonal IMB (IMB-S) developed by the Cold Regions Research and Engineering Laboratory (CRREL) is an instrument that combines the measuring principles of a sonic snow buoy and a thermistor IMB (Polashenski et al., 2011). Additionally to the thermistor string (50 mm vertical resolution), it also has an underwater sonic sensor that provides the sea-ice thickness measurements by measuring the distance from the sensor to the bottom ice surface. All sensors are sheltered in a floating elongated tube that should potentially survive summer melt and fall freeze-up processes. During N-ICE2015, in total four snow buoys, seven SIMBAs, one IMB-B, and one IMB-S provided reliable data (Table 1; Itkin et al., 2015). On *Floes 1–3*, the four snow buoys were always deployed with a colocated thermistor IMB. Additionally, on *Floe 1* and *Floe 3* the buoys were part of a larger buoy array surrounding the main ice camp that had several other IMBs deployed in remote locations 5–20 km away from the ice camp (Itkin et al., 2017). IMB-S_2015a was deployed approximately 100 km NW of *Floe 3* from where it drifted to the Fram Strait. Due to the predefined time frame for

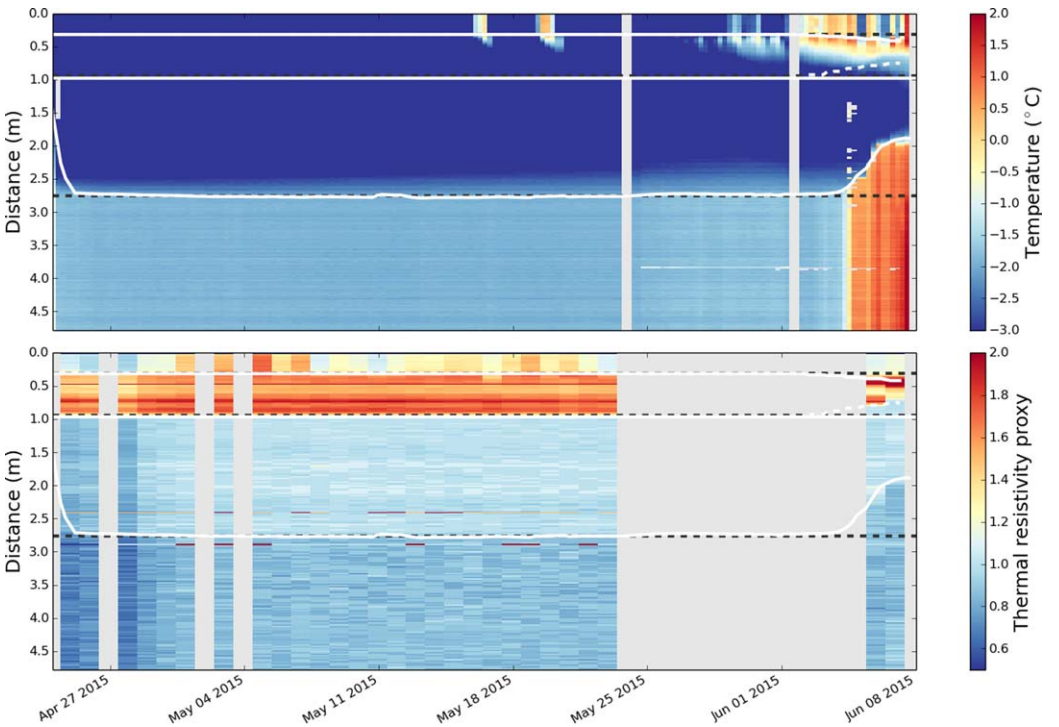

Figure 3. (a) Temperature profile and (b) thermal resistivity proxy profile for SIMBA_2015c, deployed on 24 April 2015 on *Floe 3*. The black dashed lines show initial values at deployment, the white lines overlaid are the calculated interfaces (as in Provost et al. (2017)). The dashed white line shows the surface of the slush layer, which may be transformed into a snow-ice layer. The slush layer is defined by the thermal resistivity proxy (b). The distance on the *y* axis is the distance on the thermistor chain. Toward the end of the time series bottom melt and flooding is observed. Missing or noisy data are masked as gray.

Table 1
Temporal Coverage and Initial Conditions (Measured at Time of Deployment) of IMBs, Snow Buoys, Snow Stakes, and Hotwire Fields Deployed During N-ICE2015 on All Floes

	Instrument	Type	Start date dd.mm.	End date dd.mm.	Days	Ice type	Initial snow depth (m)	Initial ice thickness (m)	Mean snow depth (m)	Mean ice thickness (m)	Δ Snow (m) per 30 days	Δ Ice (m) per 30 days
Floe 1	WAVE_2015b	Point	16.01.	23.02.	39	FYI[a]	0.15 ± 0.05	0.82 ± 0.09	n/a	n/a	n/a	n/a
	SIMBA_2015a	Point	15.01.	12.03.	57	SYI[a]	0.59 ± 0.09	1.33	0.53 ± 0.08	1.26 ± 0.12	−0.15	−0.13
	SIMBA_2015b	Point	15.01.	13.03.	58	SYI[a]	0.44 ± 0.08	1.28 ± 0.01	0.39 ± 0.04	1.33 ± 0.02	0.00	0.00
	SIMBA_2015e	Point	26.01.	23.02.	29	SYI[a]	0.21 ± 0.06	1.49	n/a	1.53 ± 0.04	n/a	−0.11
	SIMBA_2015f	Point	24.01.	17.02.	25	FYI	0.33 ± 0.14	0.90	0.51 ± 0.07	0.95 ± 0.02	0.10	0.13
	SIMBA_2015g	Point	31.01.	28.02.	29	n/a	0.41 ± 0.03	1.08	0.43 ± 0.04	1.14 ± 0.05	0.02	−0.04
	SNOW_2015a	Point	25.01.	21.02.	28	FYI	0.32 ± 0.02	0.90	n/a	n/a	n/a	n/a
	HW1/SS1	Point	23.01.	16.02.	25	FYI	0.55 ± 0.13	0.94 ± 0.10	0.57 ± 0.15	0.95 ± 0.09	0.13	0.05
	HW2/SS2	Point	27.01.	16.02.	21	FYI	0.22 ± 0.04	0.94 ± 0.04	0.28 ± 0.10	n/a	0.20	n/a
	HW3	Point	27.01.	16.02.	21	YI	0.02	0.41 ± 0.14	n/a	0.56 ± 0.10	n/a	0.23
	HW4/SS4	Point	27.01.	16.02.	21	SYI	0.36 ± 0.11	1.29 ± 0.05	0.43 ± 0.04	1.29 ± 0.01	0.10	0.00
	EM31/MP	Line i	15.01.	17.02.	34	Mixed	n/a	n/a	0.41 ± 0.19	1.47 ± 0.63	n/a	n/a
	EM31/MP	Line r	24.01.	15.02.	23	FYI	0.30	0.97	0.33 ± 0.14	0.99 ± 0.29	0.04	0.08
	EM31/MP	Line r	24.01.	15.02.	23	SYI	0.49	1.7	0.52 ± 0.12	1.73 ± 0.57	0.08	0.11
	Average *Floe 1*						0.34 ± 0.16	1.08 ± 0.33	0.44 ± 0.10	1.20 ± 0.33		
Floe 2	SIMBA_2015d	Point	07.03.	25.04.	49	SYI	0.42	1.30	0.43 ± 0.03	1.26 ± 0.02	−0.02	0.02
	SNOW_2015d	Point	01.03.	25.04.	55	SYI	0.34	1.34	0.41 ± 0.03	n/a	0.04	n/a
	EM31/MP	Line i	24.02.	19.03.	24	Mixed	n/a	n/a	0.56 ± 0.17	1.21 ± 0.87	n/a	n/a
	EM31/MP	Line r	26.02.	09.03.	14	Mixed	0.52	1.44	0.54 ± 0.19	1.23 ± 0.79	0.03	−0.08
	SS5	Point	02.03.	19.03.	18	SYI	0.36 ± 0.04	n/a	0.33 ± 0.02	n/a	−0.07	n/a
	SS6	Point	27.02.	17.03.	22	FYI	0.33 ± 0.04	n/a	0.37 ± 0.03	n/a	0.10	n/a
	Average *Floe 2*						0.40 ± 0.08	1.36 ± 0.07	0.44 ± 0.09	1.23 ± 0.03		
Floe 3	SIMBA_2015c	Point	24.04.	07.06.	45	SYI	0.61	1.79	0.60 ± 0.08	1.77 ± 0.11	−0.23	−0.38
	SNOW_2015b	Point	23.04.	07.06.	45	SYI	0.42	n/a	0.47 ± 0.02	n/a	n/a	n/a
	IMB-B_2015b	Point	08.05.	11.06.	36	YI	0.02	0.62	n/a	0.50 ± 0.10	n/a	−0.47
	IMB-S_2015a	Point	19.05.	06.07.[c]		FYI	0.28	1.05	n/a	n/a	n/a	n/a
	SNOW_2015c	Point	20.04.	11.06.	53	n/a	0.33	1.25	0.35 ± 0.03	n/a	−0.01	n/a
	SNOW_2015e	Point	21.04.	11.06.	54	n/a	0.32	1.34	0.39 ± 0.02	n/a	0.04	n/a
	EM31/MP	Line i	18.04.	05.06.	49	Mixed	n/a	n/a	0.43 ± 0.24	1.45 ± 0.82	n/a	n/a
	EM31/MP	Line r	27.04.	04.06.	42	Mixed	0.57	1.43	0.53 ± 0.17	1.56 ± 0.51	−0.03	−0.06
	HW7/SS7	Point	29.04.	04.06.	37	SYI	0.55 ± 0.17	1.47 ± 0.11	0.55 ± 0.01	1.45 ± 0.05	0.02	−0.10
	HW8/SS8	Point	04.05.	31.05.	28	SYI[a]	0.70 ± 0.10	1.08 ± 0.17	0.70 ± 0.01	1.05 ± 0.03	−0.01	−0.08
	Average *Floe 3*						0.42 ± 0.21	1.27 ± 0.33	0.50 ± 0.12	1.30 ± 0.4		
Floe 4	EM3/MP1	Line i	10.06.	18.06.	9	Mixed	n/a	n/a	0.29 ± 0.18	1.19 ± 0.52	n/a	n/a
	EM31/MP	Line r	11.06.	16.06.	6	Mixed	n/a	n/a	0.32 ± 0.20	1.36 ± 0.76	n/a	n/a
	HW9	Point	08.06.	18.06.	11	FYI[b]	n/a	1.74 ± 0.04	n/a	1.33 ± 0.41	n/a	−2.37
	Average *Floe 4*							1.74 ± 0.04	0.31 ± 0.02	1.29 ± 0.09		

Note. For sampling with EM31/Magnaprobe (MP), mean thickness is calculated from EM31 measurements, subtracted by snow depth (description in the text) and shown with standard deviation over the given period. Note that standard deviations for point measurements are temporal while they are spatial for line measurements. Line i stands for independent measurements, line r stand for repeated transect lines. The difference (Δ) is calculated from the first and the last transects on a floe and normalized to a 30 day period to make numbers intercomparable.

[a]Ice type is an estimation, derived from initial snow and ice thicknesses.

[b]Likely deformed ice.

[c]Last date where snow and ice data was transmitted, the buoy drifted into Fram Strait until 12 September 2015.

the N-ICE2015 expedition, the duration of *Floe 4* was expected to be short and since buoys would not freeze into the ice after the onset of melt, none were deployed.

3.2. Hotwires and Snow Stakes

Snow stakes and hotwire fields are commonly used and considered as low cost methods for continuous ice and snow thickness observations and used during, e.g., the SHEBA drift (Mahoney et al., 2009; Perovich, 2003). Compared with autonomous buoys they provide snow depth and sea-ice thickness at reduced temporal resolution. On the four N-ICE2015 *Floes*, we installed in total seven hotwire fields and seven snow-stake fields following the routine outlined in Perovich (2003). A rectangular hotwire field with a side length of approximately 10 m was designed in a way that in each corner a wire was installed close to an ablation

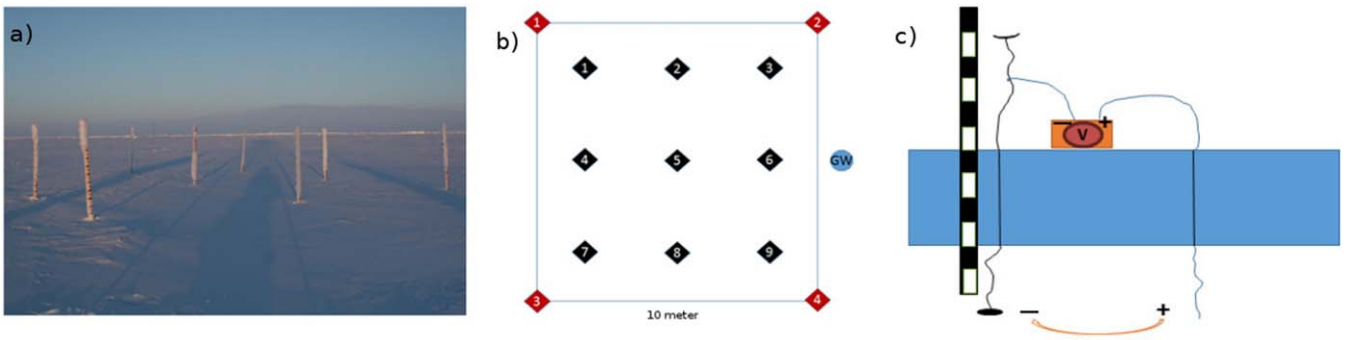

Figure 4. (a and b) Photo and schematic of a combined hotwire and snow-stake field: red squares are the positions of hotwires, blue circle is the grounding wire. Black squares show the nine snow stakes. (c) Schematic of a hotwire and the grounding wire, connected prior to the measurement to a generator.

stake, and in the middle of the hotwire field nine snow stakes with even spacing were set up (Figure 4). Snow depth and ice thickness changes were recorded on a regular basis, and the readings were averaged in space to cover small scale spatial variability (Rösel et al., 2016a, 2016b).

3.3. Spatial Surveys of Snow and Ice Thickness

3.3.1. Ground-Based Electromagnetic Surveys

Total ice and snow thickness was measured with portable electromagnetic instruments (EM31 and EM31SH, Geonics Ltd., Mississauga, Ontario, Canada) mounted on a sledge. The EM31s measure the received secondary electromagnetic field, induced by highly conductive seawater (Kovacs & Morey, 1991). Conductivity values are calibrated with drill hole measurements and postprocessed according to Haas et al. (1997). In total 101 and 145, calibration drillings were made for EM31SH and EM31, respectively, covering a thickness range from 0.15 to 4.50 m. Analysis of the calibration measurements did not reveal any drift in the fitting curve parameters on the temporal or spatial scales (see supporting information Figure S1).

The footprint size of the EM31 ranges from 3 to 5 m (e.g., Haas et al., 1997; Renner et al., 2014), depending on the ice and snow thickness. Accuracy of EM31 measurements is in the range of $\pm$0.1 m (Haas et al., 2009) for level ice, becoming higher for rough and deformed ice.

On all *Floes*, independent (i) and repeated (r) transects with combined EM31 and snow depth measurements were performed. Repeated transects are considered as repetitions of marked tracks on a weekly basis to observe temporal change, while independent transects are long surveys in different directions from the main ice camp are to cover the spatial variability of the surrounding area. One repeated transect line measurement, typically the first survey, is included in the independent data set.

3.3.2. Airborne Surveys

Helicopter-borne EM instruments (HEM) (Ferra Dynamics Inc., Mississauga, Ontario, Canada) were used to measure ice thickness in helicopter range around *RV Lance* between 15 April and 8 June 2015. Altogether, 17 HEM surveys were undertaken. The first, on 15 April, occurred while *RV Lance* was traveling into the ice to begin the drift of *Floe 3*. Sixteen surveys were carried out between 19 April and 18 May while *RV Lance* was moored to *Floe 3*. The last survey on 8 June 2015 was an overflight of *Floe 4*, operated from the *FS Polarstern's* expedition "PS92" (ARK-XXIX/1, Alfred-Wegener Institute (AWI), Bremerhaven, Germany; Peeken, 2015).

HEM measurements use the same principle as the EM31 ground surveys: They both measure the distance from the instrument to the ice bottom. The HEM uses additionally a laser altimeter to measure the height above the snow surface. The laser footprint has a diameter of about 3 cm.

The height above the bottom of the ice is derived from the strength of electromagnetic induction in the conductive water under the ice, and the height of the instrument above the surface of the ice or snow is determined with a laser altimeter (Haas et al., 2009, 2010). The difference between the two height measurements corresponds to the total thickness of ice and snow. The HEM instruments used in this study have horizontal coplaner transmitting and receiving coils spaced 2.7 m apart. They operate at a signal frequency of 4 kHz, with a 10 Hz sampling rate, corresponding to measurement point spacing of 3–5 m (Haas et al., 2009; Pfaffhuber et al., 2012). The HEM instrument is flown at a height of 15–20 m above the surface and has a

footprint of approximately 40–50 m (Haas et al., 2009). The system is calibrated by measuring at high elevations and over open water. The nominal total thickness uncertainty for a single HEM measurement is 0.1 m over level ice, with significantly larger errors and an underestimation of maximum thickness occurring in heavily ridged areas due to footprint smoothing (Haas et al., 2009; Mahoney et al., 2015).

3.4. Snow Depth Surveys

Snow depth surveys were made with a GPS snow probe, henceforth referred to as Magnaprobe (SnowHydro, Fairbanks, AK, USA). The Magnaprobe is a thin pole with a sliding disk of 0.2 m in diameter around it. The pole penetrates the snow pack to the sea-ice surface while the disk rests on the snow surface. Inside the pole a magnetic device measures the distance between the disk and the lower tip of the pole providing the snow depth (Sturm & Holmgren, 1999). Each depth is time-tagged and position-tagged and recorded on a data logger. The Magnaprobe enables snow depth surveys with several thousand snow depth measurements in a few hours. The accuracy of the measurement is ± 3 mm (Marshall et al., 2006) and the footprint is the size of the disk.

3.5. Merging of Electromagnetic Soundings and Magnaprobe Measurements

For direct comparison of the values, and to subtract the snow depth from the EM31 data, we resampled the EM31 data onto the coordinates of the Magnaprobe track, and we applied a Gaussian filter to the EM31 data. The EM31 and Magnaprobe data sets (Rösel et al., 2016c, 2016d) were median-sampled on a 5 m regular grid, following the approach by Geiger et al. (2015). Snow depth was subtracted from the EM31 values to derive sea-ice thickness. To facilitate this regridding, both the Magnaprobe and EM31 data were corrected for sea-ice drift. The drift correction routine is based on subtraction of the floe track over the period preceding the exact timing the measurement was carried out. Starting from the second position of the instrument in the particular measurement sequence, the Global Navigation Satellite System (GNSS) station coordinates were used to calculate the back trajectories of the measurement points with respect to initial time of the series.

The floe track itself is computed using the data from one of two GNSS base stations (called hereafter GPS1 and GPS2) that were installed on the ice stations, or the Lance position when the base stations were not in operation. Note the approach we use implicitly assumes that rotation of the floe over the measurement period was negligible. This is reasonable since EM31 and Magnaprobe measurements were always carried out at the same time with a maximal time lag of 30 s. The single point horizontal accuracy for such floe position measurements varies in time being of the order of 1–4 m. For those measurements, where single point accuracy was critical, such as, e.g., validation fields for airborne campaigns, the data were postprocessed using Precise Point Positioning (PPP) processed reference tracks of GPS1 and GPS2. This increases the track accuracy to 0.2–0.3 m and takes the rotation of the floes into account. The PPP processing was performed by using the open source RTKLIB software package (http://www.rtklib.com).

In order to avoid oversampling for the survey periods when the instrument was stationary relative to the ice, we estimated the instrument velocity from the drift corrected measurement positions and eliminated the values corresponding to instrument speeds below 0.2 m s^{-1}.

3.6. Drill Hole Measurements and Freeboard Calculations

3.6.1. Drill Hole Measurements

During the N-ICE2015 expedition, we obtained more than 400 direct measurements from drill holes or holes from ice coring on different types of level ice. They are arbitrarily located in the vicinity of the snow and ice thickness transects, within a 5 km radius around the ship. For measuring freeboard at the drill holes, first snow thickness is measured above the drill hole, afterward snow is removed and the hole is directly drilled or cored into the sea ice. The thickness is measured with a flexible thickness gauge with a foldable metal piece at the bottom as weight. The distances from the ocean-ice interface to both the water surface and the ice surface are noted. We estimate the uncertainty of these measurements to be less than ± 0.02 m, resulting from the sampling uncertainties such as, i.e., different observers, differences in reading of the tape, different strength of pulling the tape, or uneven bottom of the sea ice. More than half of the thickness drillings are used for the calibration of electromagnetic measurements (see section 3.3.1). Drill hole measurements provide spatial ice and snow thickness as well as freeboard and draft information at point scale, but without temporal component (Rösel & King, 2017).

3.6.2. Freeboard Calculations

Freeboard values h_{fb} can either be read directly from tape measurements at drill holes, or they can be calculated based on the principle of an isostatic equilibrium (Forsström et al., 2011):

$$h_i = \frac{\rho_w}{\rho_w - \rho_i} h_{fb} + \frac{\rho_s}{\rho_w - \rho_i} h_s \quad (1)$$

where ρ_w is 1,027 kg m^{-3} (Meyer et al., 2017b). For winter conditions (*Floe 1* and *Floe 2*), the bulk density of the snow pack is $\rho_s = 345 \pm 39$ kg m^{-3}, bulk density for FYI is $\rho_i = 910 \pm 18$ kg m^{-3}. For spring conditions (*Floe 3* and *Floe 4*) we define $\rho_s = 313 \pm 50$ kg m^{-3} and $\rho_i = 901 \pm 18$ kg m^{-3}; density values are extracted from snow pits (Gallet et al., 2017; Merkouriadi et al., 2017b) and ice core analysis (Gerland et al., 2017). For snow depth h_s, we used Magnaprobe measurements and for ice thickness h_i, we used the values obtained from the combination of EM31 and Magnaprobe data. In this study, we analyze calculated freeboard from long independent walks. By using equation (1) we have to take into account that we might get results with an offset toward higher freeboard values in case of flooding, because ρ_s of a flooded snow pack will be substantially higher.

4. Results

The combined sea ice and snow thickness data from all different sources is summarized in Table 1, providing an overview about the temporal and spatial variability of snow and ice thickness during the entire N-ICE2015 expedition.

Independent snow and ice thickness transects from combined EM31/Magnaprobe measurements give average values, including standard deviations, in the range from 1.19 ± 0.52 to 1.47 ± 0.63 m for ice and 0.29 ± 0.18 to 0.56 ± 0.17 m for snow, for all the floes (Table 1). Average values of ice and snow thickness from point measurements and their evolution throughout the entire N-ICE2015 expedition from January to June 2015 are shown in Figure 5.

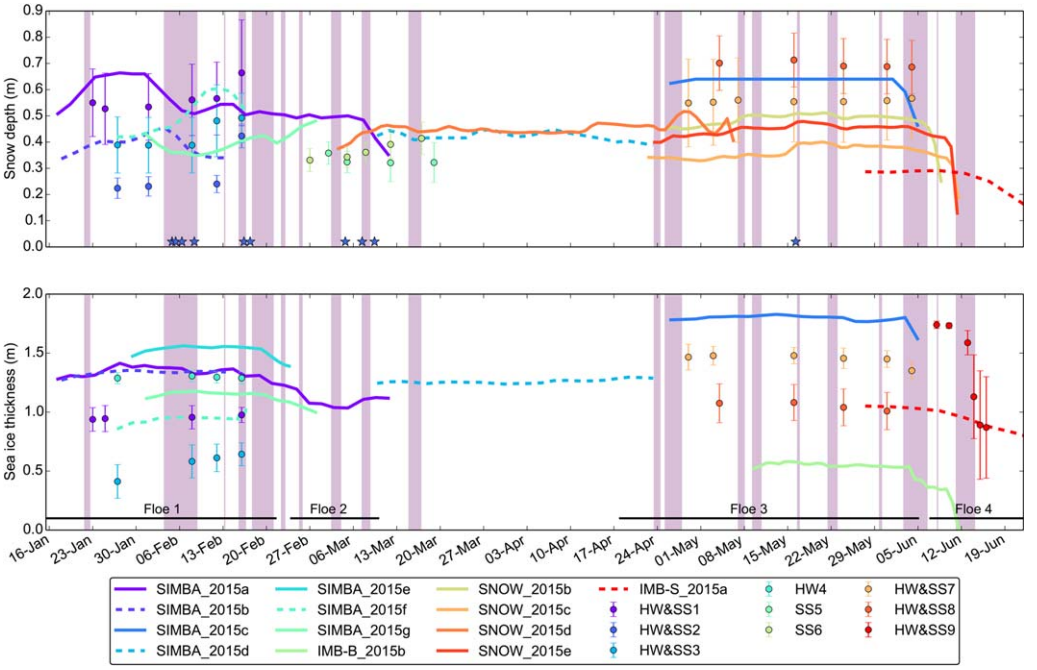

Figure 5. (a) Snow depth and (b) sea-ice thickness, extracted from IMBs, snow buoys, snow-stake fields (SS), and hotwire fields (HW) during N-ICE2015. The error bars represent the standard deviations. The purple shading in the background indicates storm events, labeled as M (major) and m (minor) storms according to Cohen et al. (2017). The stars show major snow fall events (Cohen et al., 2017). Note that before 2 February 2015 no precipitation data, and between 18 March and 18 April 2015 no wind speed and no precipitation data are available.

4.1. *Floe 1*: 15 January to 21 February 2015

The data acquired by five IMBs, a snow buoy, hotwire, and snow-stake fields associated with *Floe 1* and its surrounding represent different snow and ice conditions observed during the drift. All buoys show a weak increase in ice thickness during a period of low air temperatures in the last week of January, followed by an increase of snow depth from 0.59 to 0.66 m for SIMBA_2015a and a decrease from 0.45 to 0.35 m for SIMBA_2015b (Itkin et al., 2015). During a major storm event lasting from 3 to 8 February (M2) (Cohen et al., 2017), snow depth at SIMBA_2015b and SIMBA_2015g decreased, while it increased at SIMBA_2015e. SIMBA_2015a, SIMBA_2015f, and SIMBA_2015g show both: first an increase and later a decrease of snow depth (Figure 5). The decrease in snow depth can be explained by blowing snow and its redistribution. It should be noted that these are point measurements and they do not capture the spatial variability of the snow.

While drifting over Atlantic Water in mid-February (Meyer et al., 2017b) the southernmost buoy SIMBA_2015a (20 km distant from *Floe 1*) indicates bottom melt starting on 16 February, followed by a similar signal from SIMBA_2015e and SIMBA_2015g starting on 19 February (Figure 5). Initial flooding with a gradual snow-ice formation on the snow/ice interface was observed at SIMBA_2015a (Figure 5; Provost et al., 2017). Due to ice temperatures of -4.5°C we surmise that the ice was permeable (Weeks & Ackley, 1986), and negative freeboard promoted snow-ice formation on SIMBA_2015a. During the last week of February and the first week of March, ice breakup events, flooding, and subsequent snow-ice formation led to a rapid decrease of snow depth and an increase of ice thickness. On 18 February, a deformation event led to lateral flooding of *Floe 1*, and subsequent snow-ice formation was observed in the SIMBA_2015f record (Provost et al., 2017).

From the hotwire and snow-stake fields HW1&SS1 (FYI) and HW4&SS4 (SYI) initial ice thicknesses with standard deviations were 0.94 ± 0.1, and 1.29 ± 0.05 m, respectively (Table 1). The last readings 4 weeks later showed values of 0.98 ± 0.06, and 1.30 ± 0.05 m, respectively. Only hotwire field HW3, deployed in a refrozen lead with an initial snow cover of 0.02 m showed a significant increase from 0.41 ± 0.14 to 0.64 ± 0.09 m (Table 1 and Figure 5). The initial snow depth with standard deviation at the SYI field was 0.55 ± 0.13 m, and about 0.16 m higher than at the FYI field with an initial observed snow depth of 0.39 ± 0.11 m. On both ice types the snow depth showed a net increase of about 0.1 m within 1 month.

Figure 6a presents *Floe 1* ice and snow thickness probability density functions (PDF) derived from independent measurements with EM31 and Magnaprobe. Note, that in Figure 6, all distributions represent both spatial and temporal variability since spatial data from a longer period are included. The PDF of the ice thickness features a trimodal distribution with a first peak at 0.3 m corresponding to thin ice, a second peak at 0.9 m, and a third major peak, which represents the primary mode at 1.5 m. Mean ice thickness was 1.47 m with a standard deviation of 0.63 m. The tail of the PDF above 1.8 m represents deformed ice.

The modal ice thickness for all repeated FYI transects was 0.80 m (Figure 6b). The modal thickness for all repeated SYI transects was 1.40 m. On FYI, the average snow depth with standard deviation was 0.33 ± 0.14 m, whereas on SYI, it was 0.52 ± 0.14 m (Figure 6b). The distributions of both snow depth and ice thickness do not differ greatly over either type between the first and last transect lines. We notice a shift from the FYI mode from 0.8 to 0.9 m and for the SYI mode from 1.5 to 1.6 m, but the averages for both ice types for the first and the last transect stayed in the same order of 1 m for FYI and 1.8 m for SYI. The mode for snow thickness on FYI increased by 0.05 m from 0.20 to 0.25 m on FYI while it decreased by the same amount from 0.60 to 0.55 m on SYI.

4.2. *Floe 2*: 24 February to 19 March 2015

On *Floe 2*, snow buoy SNOW_2015d, SIMBA_2015d, and snow-stake field SS5 were deployed together on SYI at the main ice camp. Initial snow depth for SNOW_2015d was 0.34 m (Table 1). The buoy showed an increase of 0.15 m in snow depth after deployment, caused by two major storm events (M4 and M5) with precipitation (Cohen et al., 2017). SIMBA_2015d was deployed 1 week later, after the storm, with initial snow and ice thicknesses of 0.42 and 1.30 m, respectively. During the drift, we registered only slight variations in the range of a few centimeters in snow depth and ice thickness (Figure 5). The snow-stake field on FYI (SS6) showed an increase from 0.33 to 0.41 m while the snow stakes on SYI (SS5) showed a decrease from 0.36 to 0.32 m (Figure 5).

The thickness distributions for the independent measurements and the repeated transect lines (Figures 6d and 6e) on *Floe 2* show similarities: the thin ice class with ice thickness values in the range from 0.0 to 0.3 m is present in both histograms. The main modal peak is around 1.0 m, representing the fraction of

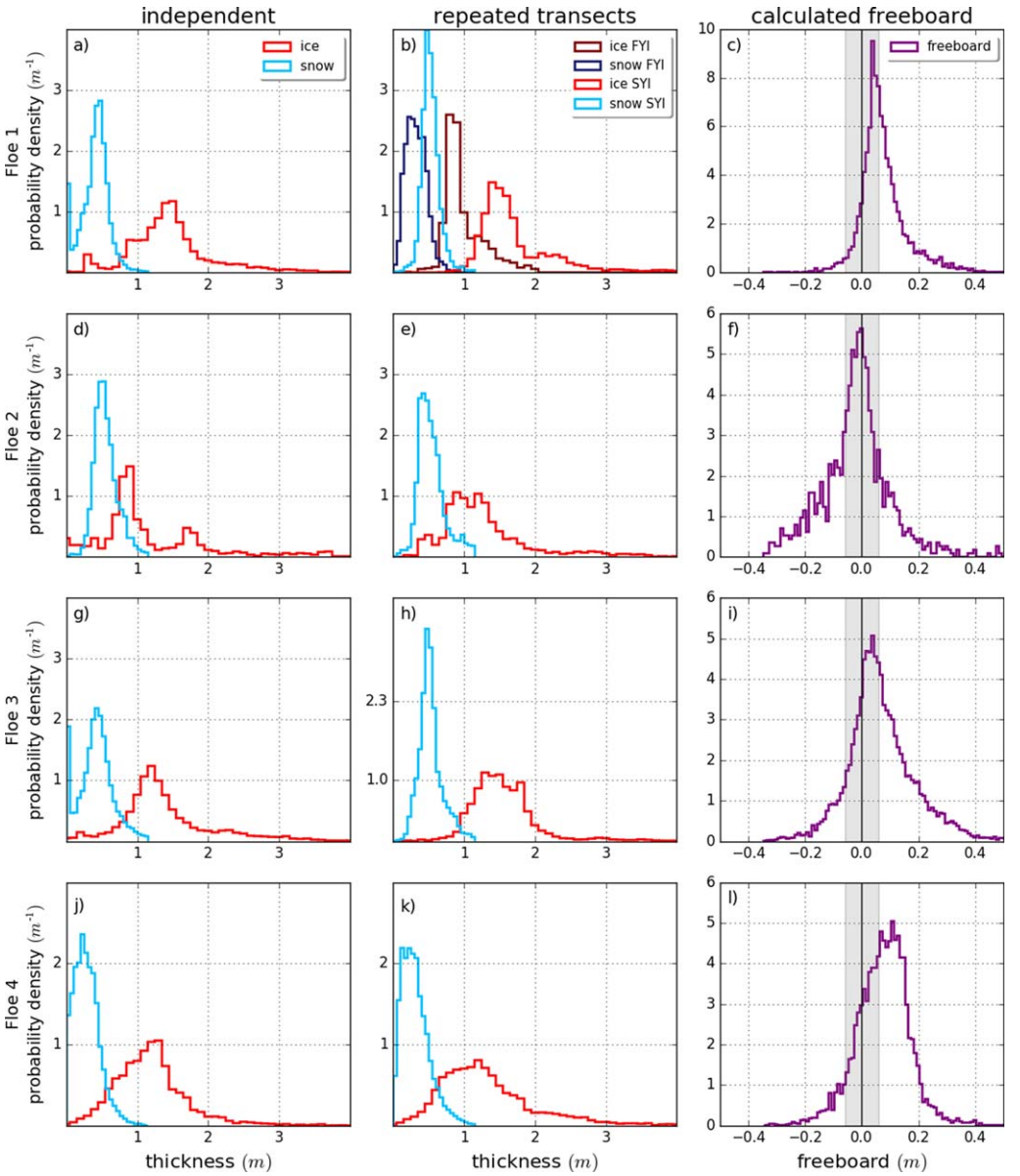

Figure 6. Snow and ice thickness distributions from (left) independent measurements and (middle) repeated measurements for all *Floes*. SYI and FYI is only distinguished for *Floe 1* on all repeated transects, for *Floes 2*, *3*, and *4* the distributions contain a mixture of SYI and FYI. The right column displays calculated freeboard from the independent measurements of each floe. The gray shaded areas indicate the values that fall in the uncertainty range of ± 0.06 m based on ± 1 STD. The bins in the pdfs are centered and bin size for ice thickness is 0.10 m, for snow depth 0.05 m, for freeboard 0.01 m. All distributions represent both spatial and temporal variability.

dominating FYI. For the transect lines, a third mode can be identified at 1.3 m, whereas in the independent measurements, a third mode is at 1.8 m. The snow depth with standard deviation on *Floe 2* from independent measurement is comparable to the measurements on the transect line and the mean is 0.55 ± 0.18 m (Figure 6d). On *Floe 2*, the conditions were quite stable; the average thickness of ice and snow did not change within 3 weeks of the drift on this floe (Table 1). Snow depth on FYI and SYI was in the range of 0.33–0.56 m (Table 1), but it is not distinct that the values in the higher range always correspond with SYI.

4.3. *Floe 3*: 18 April to 5 June 2015

The IMBs, snow-stake, and hotwire fields on *Floe 3* show coinciding results throughout the drift. During the first 4 weeks after the installation of the snow-stake and hotwire sea-ice and snow conditions remained

stable around 1.08 and on 1.47 m on SYI with 0.70 and 0.55 m of snow. This is confirmed by the data from SIMBA_2015c, which had an initial ice thickness of 1.79 m with 0.61 m snow. Starting at the beginning of June, rapid bottom melt with a rate of about 0.10 m d^{-1} commenced on both ice types, while the snow depth remained unchanged. SIMBA_2015c shows an indication of a weak basal melt already after 25 May followed by a steep increase of the basal melt rate on 5 June (Figure 3). Subsequent freeboard adjustment and flooding of the floe caused the formation of a slush layer with a thickness of up to 0.30 m (Figure 3). Due to the high density and the salinity of the slush layer and its potential to refreeze, we will here consider the slush layer as sea ice. Observed 2 m air temperatures well below 0°C until 1 June (Hudson et al., 2015) and also cold sea-ice temperatures may allow the slush layer to refreeze subsequently to a snow-ice layer. Consequently, snow depth measured by SIMBA_2015c gradually decreased, starting at the end of May. The next significant decrease in snow depth registered in early June by the three snow buoys is connected to storm events (Figure 5: M8 on 2–6 June and m9 on 8 June; Cohen et al., 2017), and might be caused by lateral flooding induced by breakup events of *Floe 3*. Note, that snow buoys can only measure the change of the distance from the snow surface to the sensor, which was in this case an increase and might be a sign of compacting snow. Flooding or snow-ice formation cannot be detected by snow buoys. IMB-B_2015b was deployed on 8 May in a refrozen lead about 20 km NW of *RV Lance* with initial ice thickness of 0.62 and 0.02 m of snow. This is below the detection limit of the thermistor chain, so no snow depth can be shown in Figure 5. A gentle decrease of ice thickness from the bottom can be observed already after 16 May, followed by a sharp increase of the basal melt rate on 5 June that continued until complete disintegration of the level ice on 12 June, 20 km from the open water (Figure 5). IMB-S_2015a was deployed on 19 May on level FYI with initial thicknesses of 1.05 m for ice and 0.28 m for snow, respectively. IMB-S_2015a showed no sign of snow-ice formation. Ice and snow thickness both decrease gradually in June, caused by bottom melting and snow melt or compaction.

The repeated measurements on *Floe 3* also showed stable conditions in terms of snow and ice thickness until the onset of gradual melt in the second half of May. Then both snow and ice thickness show a decrease in thickness (see Table 1). The comparison of the first and the last repeated transect line results in an average decrease of 0.16 m in ice thickness and 0.02 m in snow thickness. The sea-ice thickness distribution of *Floe 3* is bimodal, with a first mode at 1.2 m and a second mode at 0.2 m, which represents a large refrozen lead in the vicinity of the ship (Figure 6g). Connected to these two distinct sea-ice modes, the observed snow depth distribution shows a peak at 0.03 m representing the snow cover of the refrozen lead. The second mode is at 0.45 m associated with the snow cover on FYI and SYI. Figures 6g and 6h demonstrate that the distributions from the independent measurements and the repeated transect lines are comparable, except for the mode corresponding to the snow on thin ice only present in the independent measurements.

4.4. *Floe 4*: 7 to 22 June 2015

Floe 4 was established on FYI within the marginal ice zone. At the hotwire field HW9, an intense bottom melting event was observed, which started between 10 and 13 June, with melt rates up to 0.25 m d^{-1} (Figure 5). This hotwire field was in a deformed area of the floe, therefore may not be fully representative of processes on level ice. We assume the ocean induced melting of deformed ice could lead to disintegration of previously consolidated ice blocks efficiently accelerating the melt process.

The snow and ice distributions for *Floe 4* both show an unimodal distribution, where the mode for snow is located at 0.20 m and for ice at 1.25 m (Figures 6j and 6k). The comparison of independent measurements with repeated transects shows that the transect lines represent well the overall surrounding (Table 1). On *Floe 4*, the established survey line could not be followed due to strong bottom melt and a rapid transition from solid into rotten ice, making a quantitative intercomparison of the entire surveys difficult. However, we found a decrease of the average sea-ice thickness of 0.5 m within 10 days when we compare the first and the last transect line. This might also explain the wider thickness distributions for *Floe 4*. The snow thickness decreased by 0.05 m. In general, a flooding of vast parts of *Floe 4* was registered after 14 June, along with formation of a snow-ice crust in wet snow (see Figure 7) above the flooded snow pack. This ice layer grew over several days toward the former snow/ice interface. The formation of this crust resulted in a sudden decrease of snow depth and the same amount of increase in ice thickness; we noted that in many areas the Magnaprobe pole could not penetrate through the crust to the original snow/ice interface and might bias the observations.

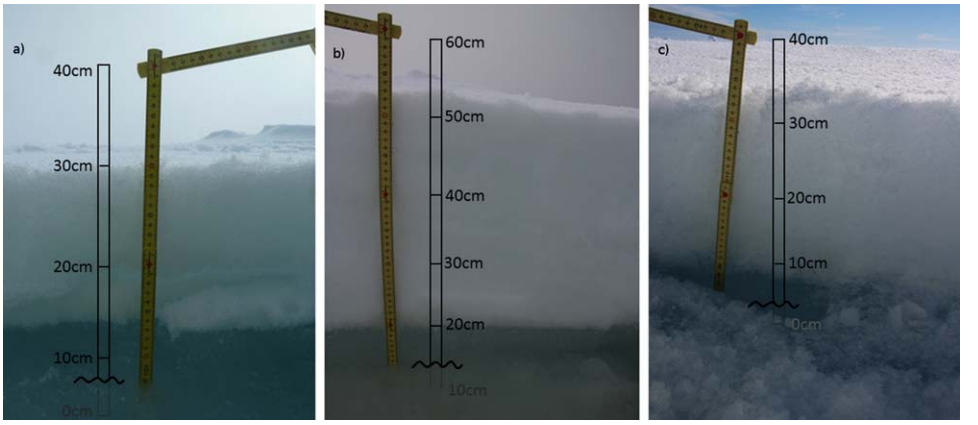

Figure 7. Snow pits with flooded snow pack on *Floe 4* on 14 June 2015 on three different sites. (a) Close to the ship, water level at 0.075 m, wet snow until 0.14 m, total snow depth 0.30 m. (b) Water level at 0.13 m, wet snow until 0.19 m, total snow depth 0.53 m. (c) Water level at 0.06 m, wet snow until 0.09 m, total snow depth 0.34 m.

4.5. Regional HEM Surveys Over *Floe 3* and *Floe 4* Surroundings

Figure 8 presents all HEM surveys including date and time (King et al., 2016); basic statistics for each survey are summarized in Table 2. The total snow and ice thickness distribution for all HEM surveys combined has mode 1.7 m and mean 1.8 m. There is a second mode at between 0.1 and 0.3 m in almost all the surveys that is representative of the thin ice class found in refrozen leads.

Long HEM surveys toward the east on 6 and 12 May show a distribution dominated by the thin ice class, while flights along the main drift direction show very little variation between the surveys.

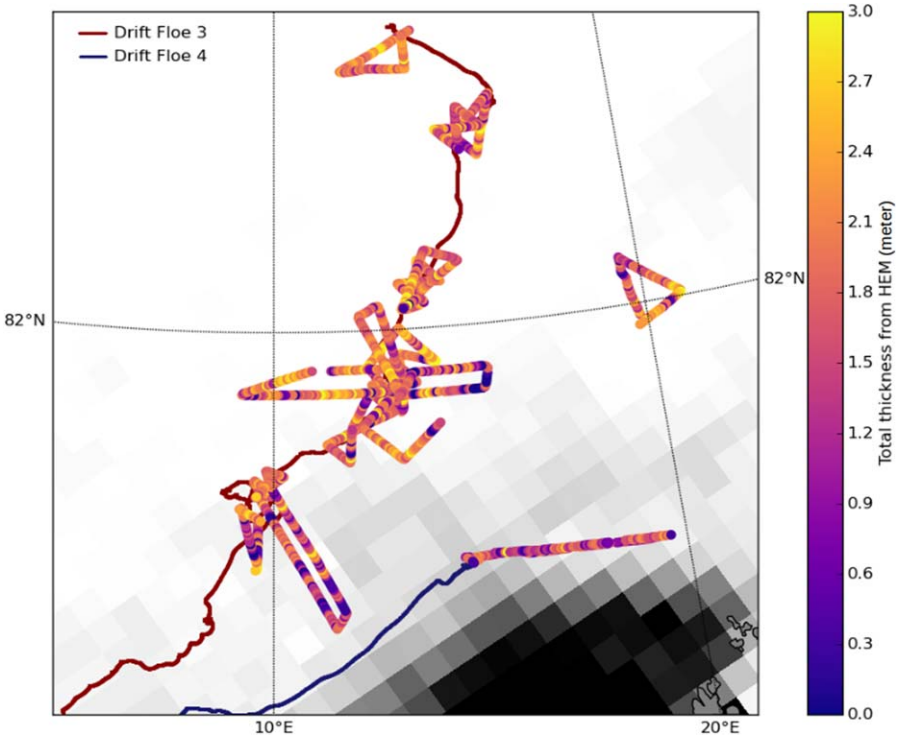

Figure 8. HEM surveys carried out in the N-ICE region between 15 April and 8 June 2015. The flight at 82°N/20°E was a reconnaissance flight on the way the start position of the third drift. The background is sea-ice concentration (black is 0%; white is 100% sea-ice concentration) from 15 May 2015 based on SSM/I data, calculated with ASI algorithm, provided by ICDC, University Hamburg.

Table 2
Total Snow and Ice Thickness From HEM Surveys

Date	Start lon/lat	Thickness mode (m)	Thickness mean (m)	Notes
15 Apr 2015	19.81/81.95	1.9 (0.1)	1.8 ± 0.9	Reconnaissance flight
19 Apr 2015	14.26/83.15	1.8	2.1 ± 0.8	
24 Apr 2015	15.37/82.75	1.7 (0.1)	1.7 ± 0.8	Local area survey
24 Apr 2015	15.30/82.73	1.7 (0.3)	1.8 ± 1.0	
28 Apr 2015	13.96/82.18	1.8 (0.1)	1.8 ± 0.9	Local area survey
29 Apr 2015	13.57/82.07	1.5	1.9 ± 1.0	
30 Apr 2015	13.30/82.00	1.9 (0.2)	2.1 ± 1.1	
05 May 2015	13.20/81.80	1.7 (0.2)	1.6 ± 0.9	Local area survey
05 May 2015	13.43/81.79	1.7 (0.3)	1.9 ± 0.9	
05 May 2015	13.23/81.77	1.8 (0.2)	1.9 ± 1.0	
06 May 2015	13.32/81.76	1.8 (0.1)	1.9 ± 1.0	
06 May 2015	13.13/81.79	0.1 (1.8)	1.4 ± 1.0	Long track east
08 May 2015	12.03/81.63	1.7 (0.1)	1.7 ± 1.1	
11 May 2015	9.85/81.40	1.5 (0.3)	1.8 ± 0.8	
12 May 2015	9.53/81.36	0.3 (1.3)	1.4 ± 1.0	Local area survey/buoy overflight
18 May 2015	9.61/81.28	2.0 (0.1)	1.6 ± 1.1	Long track south-east
08 Jun 2015	19.30/81.10	1.4 (0.1)	1.5 ± 0.9	
All flights		1.7 (0.1)	1.8 ± 0.9	

Note. Times are UTC. Second mode in brackets is included where one exists. Mode and mean thickness with standard deviation for all surveys from *Floe 3* and *Floe 4* are calculated from all of the data points.

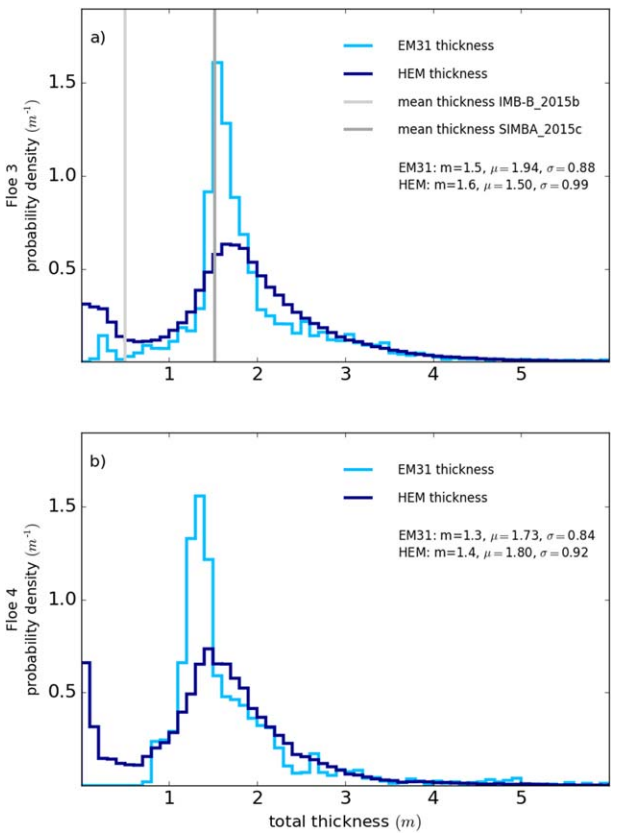

Figure 9. (a) Probability density functions of all independent EM31 and HEM ice and snow thickness measurements during *Floe 3* (April–early June 2015). Average ice thickness from buoys SIMBA_2015c and IMB-B_2015b are marked by a black line. (b) Probability density functions of independent EM31 and HEM ice and snow thickness measurements from AWI flight on 8 June 2015 over *Floe 4*.

Four local area surveys with a radius of 10 km around the ice station were carried out on a repeated pattern over *RV Lance*'s position on 24 and 28 April and on 5 and 11 May. Between the 28 April and 5 May an increase of the second mode from 0.1 to 0.2 m can be observed, indicating a thickening of the YI. The primary mode ranges between 1.7 and 1.8 m. The local survey on 11 May did not follow exactly the pattern of the previous three surveys due to bad weather. The ice thickness distribution of this flight has a primary mode at 1.5 m and a weak second mode at 0.3 m.

The HEM flight on 8 June over *Floe 4* shows a slightly thinner sea-ice cover with a mode at 1.4 m and a mean thickness of 1.5 m.

4.6. Comparing Airborne With Ground-Based EM Data

The independent EM31 data set agrees well with HEM measurements in the vicinity of *Floe 3* made from mid-April until mid-May (Figure 9a). Both PDFs show a bimodal distribution with the major peak in the thicker level ice, and a second mode, representing the thin ice. The thin ice mode is less pronounced in the EM31 data, because for safety reasons it was difficult to collect data of ice thickness in newly refrozen leads. This under-representation of very thin ice also explains the slightly higher mean values of ice thickness derived from the EM31 data.

As strong bottom melting resulted in a remarkable thinning on *Floe 4* only two EM31 surveys on 10 and 11 June can be compared with the HEM survey from 8 June. The modes for both distributions are at 1.3 m, the mean for EM31 is 1.7 m, and for HEM 1.5 m (Figure 9b). On *Floe 4*, no thin ice or refrozen lead was present in the area of the ice station, but in the larger vicinity, which was covered by the HEM survey on 8 June (Figure 9b).

4.7. Freeboard During N-ICE2015

On all four floes widespread negative freeboard along with flooded areas was observed from the drilling records: 32% (*Floe 1*), 37% (*Floe*

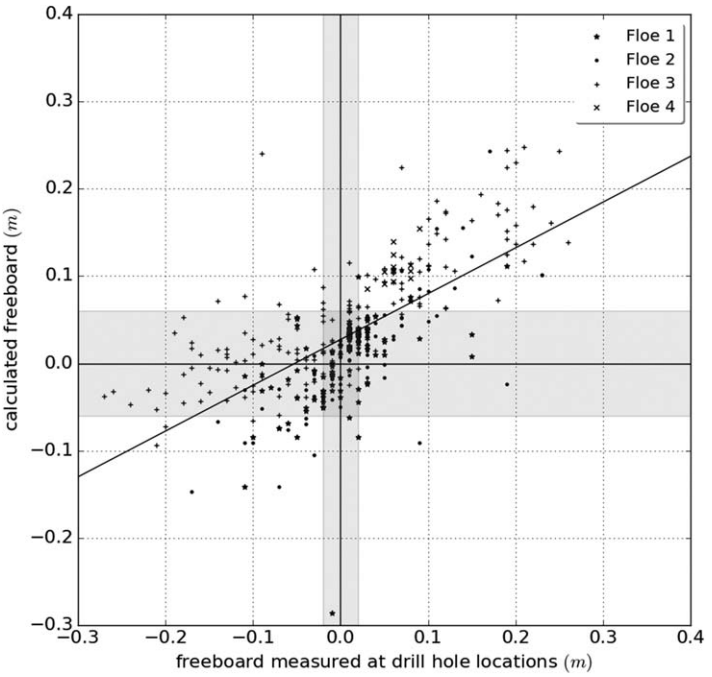

Figure 10. Scatterplot of freeboard measured in situ at drill holes (Rösel & King, 2017) versus the calculated freeboard using equation (1) for all four floes. The uncertainties based on ±1 STD of ±0.02 m for measured freeboard and ±0.06 m for calculated freeboard around 0.0 m are shaded light gray.

2), 61% (*Floe 3*), and 48% (*Floe 4*) of the readings show negative freeboard, considering an uncertainty of ±0.02 m for the measured freeboard. All values within this range (in total 31%) were discarded. We consider the drill holes to be representative for the area, because they are numerous (N = 475) and arbitrarily located. In addition, we have calculated freeboard from snow and ice thickness measurements of the long independent walks referring to the method in section 3.6.2 (Figures 6c, 6f, 6i, and 6l). Considering an uncertainty of ±0.06 m, the calculated negative fraction of freeboard on all four floes is 5% on *Floe 1*, 62% on *Floe 2*, 18% on *Floe 3*, and 11% on *Floe 4* (Figure 6).

We estimate the uncertainty of the calculated freeboard resulting from the propagation of uncertainties in the snow and ice densities and the sampling uncertainty (represented by the spatial variability) to be on average ±0.06 m. For calculated freeboard considered as a function of h_i, h_s, ρ_i, and ρ_s, at every analyzed location, the freeboard absolute uncertainty is calculated as a square root of the sum of squared partial increments of this function due to errors in the input variables. We used as measurement error the standard deviations of ρ_i, and ρ_s, and for h_i and h_s we used their observed standard deviations, since the sampling uncertainty, represented here by the standard deviation of snow and ice measurements, is a better approximation of the large areal impact on freeboard than the measurement error of each individual point. We consider the errors in the four measured variables of the error propagation method to be independent, because they were derived by different methods. The comparison of observed freeboard to calculated freeboard from drill hole measurements (Figure 10) gives an overall agreement with a correlation of $r^2 = 0.49$, but it also shows significant scatter. With regard of the uncertainty of ±0.02 m for the measured freeboard, 40% of the drill hole values lie above the uncertainty, 29% lie below and 31% of the values fall within the range of uncertainty. For the calculated freeboard, a 73% of the values from the independent long walks lie within the uncertainty range of ±0.06 m, while only 5% lie below and 22% lie above.

It is also noticeable that the correlation is higher for a positive freeboard than for negative freeboard. The scatter might be caused by the fact that individual locations for the drill holes are not always at isostatic equilibrium since internal pressure in the ice might cause a certain disturbance. In addition, the calculations appear to underestimate negative freeboard, where the snow load can cause flooding of the snow layer which results in a higher density of the snow pack. Additionally, the measurement error for negative freeboard values might be higher because the interfaces, especially for water and snow are difficult to distinguish after flooding.

4.8. Snow Melt on *Floe 3* and *Floe 4*

Events of snow melt were observed on both *Floe 3* and *Floe 4*. Temperatures rose to 0°C twice in May, but we observed no change in the snow depth in connection with these events. The onset of intense snow melt on *Floe 3* was registered on 4 June when the 2 m air temperature exceeded 0°C and stayed around the freezing point with slight variations due to the diurnal cycle (Cohen et al., 2017; Hudson et al., 2015).

On *Floe 4*, we observed a darkening of the snow cover in depressions in the vicinity of pressure ridges on 8 June, which was an indication of a continuous wetting of the snow pack. Air temperature remained above freezing between 8 and 9 June promoting melt pond formation in these dark spots. Air temperature dropped again below 0°C on 10 June. Distinct signs of snow surface melting due to radiative forcing with a rapid transformation of the crystal structure of the snow pack on a large scale was observed on 14 June, when the 2 m air temperature increased again to 0°C (Gallet et al., 2017). Additionally, snow pit and ice core temperature data gave evidence of an isothermal temperature profile through the entire snow and ice pack, along with increasing bulk snow densities (Gallet et al., 2017; Gerland et al., 2017; Merkouriadi et al., 2017b).

5. Discussion

This compilation of the N-ICE2015 snow and sea-ice thickness data sets (Rösel et al., 2016a, 2016b, 2016c, 2016d) represents a unique opportunity to study and understand processes in the winter-to-spring evolution of a thinner sea-ice cover with a thick snow cover from the Atlantic sector of the Arctic from winter conditions to melt onset.

5.1. Sea Ice During N-ICE2015

The N-ICE2015 expedition took place over the Nansen Basin and the Yermak Plateau, in an area where the Arctic Ocean is connected to the Atlantic Ocean via the deep Fram Strait and the shallow Barents Sea (Meyer et al., 2017b). The exchange of northward flowing warm and saline Atlantic Water and southward cold Arctic water near the surface gives in combination with the bathymetry makes this region special in terms of heat exchange. The shallow Yermak Plateau is a local hot-spot for vertical mixing and cooling of Atlantic Water, while in the deep Nansen Basin the cold Polar Water dominates (Meyer et al., 2017b). Also, the Atlantic Ocean and the Fram Strait is a prominent pathway for low pressure systems which penetrate across the North Pole and cause winter warming events in the Central Arctic (Graham et al., 2017b; Rinke et al., 2017).

Our observations show that during N-ICE2015, interaction at the ocean-sea-ice interface was determined to be the most significant factor driving the ice thickness changes, because thick snow moderated the influence from the atmosphere. During winter negative heat fluxes (Meyer et al., 2017a) caused a slight increase of sea-ice thickness. This increase in thickness was especially pronounced in areas with thin snow cover, e.g., refrozen leads or new ice (Table 1). However, the sea-ice growth is moderated by the insulating effect of the snow cover. The thick snow pack of on average 0.52 ± 0.18 m on SYI on *Floe 1* in January and February, during the coldest period of the experiment, limited thermodynamic ice growth (Provost et al., 2017). When the station drifted over warm Atlantic Water a significant reduction of ice thickness due to bottom melt was observed. In particular, we registered such events once in winter on *Floe 1*, starting on 17 February at 82°N, and twice in spring: on *Floe 3*, 4–5 June at 80°N, and on *Floe 4*, 12–18 June at 80°40′N (Meyer et al., 2017a). Both bottom melting events, during *Floe 3* and *Floe 4* were associated with a strong positive ocean heat flux up to 400 W m^{-2} in the mixed layer at the ocean-ice interface, driven by a combination of shallow Atlantic Water and storm events (Meyer et al., 2017a; Peterson et al., 2017). The combination of positive ocean heat fluxes with storm events or strong swell induced by storm events caused the breakup of the aforementioned floes (Itkin et al., 2017).

From the analysis of multimodal total thickness distributions from EM31 transects on *Floe 1* and *Floe 2*, we can clearly differentiate between level YI, FYI, SYI, and deformed thick ice. This is, however, not the case on *Floe 3*, where the modes associated with FYI and SYI are no longer distinct. A similarity in total ice thickness distributions for both ice types is also confirmed by the drill hole and ice core measurements. From *Floe 3* onward, the analysis of total thickness distributions alone is not sufficient for a robust classification of sea-ice types, which then requires, e.g., ice core analysis (Granskog et al., 2017).

5.2. N-ICE2015 in the Context of Other Studies in the Region

In line with pan-Arctic trends, a shift to a thinner Arctic sea ice during the transition from winter to summer in the last decade in the study region has been already shown in Renner et al. (2013). The comparison of the N-ICE2015 HEM surveys with HEM surveys in the same region from April 2009 and April–May 2011 (Haas et al., 2010; Renner et al., 2013) revealed a decrease of the mode of total thickness from 2.4 m in 2009 over 1.8 m in 2011, down to 1.7 m in 2015. It should be mentioned that most of the N-ICE2015 surveys were further north than the flights in the previous years at the same time of the year.

Between 83°N and 81°N no gradient was observed in ice thickness. A gradient toward a thinning of the sea-ice cover occurred from 81°N southward. This expected gradient is associated with warm Atlantic Water influence on the ice pack which consequently results in a breakup of floes and rapid melting. According to historical observations in the region (e.g., Renner et al., 2013), this process is generally limited to the area within a distance of 50 km to open water, which is also shown by the two southernmost HEM flights from 12 May and 8 June 2015 having with 1.5 and 1.4 m, respectively, the lowest modal thickness.

Interannual variability of snow and ice thickness is significant on a range of spatial and temporal scales (Figure 11). During N-ICE2015 the observed regional ice thickness was reduced and the snow depth was higher

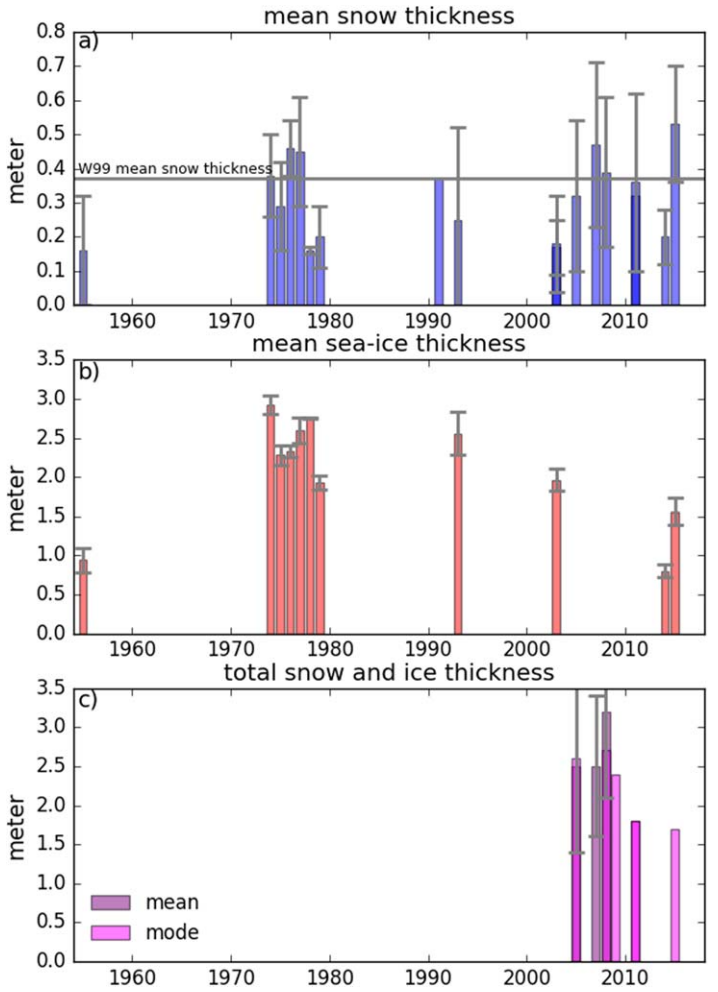

Figure 11. (a) Mean snow thickness, (b) mean sea-ice thickness, and (c) mean and modal total thickness values from historical and recent observations in the area north of Svalbard, as listed in Table 3. The error bars present the standard deviation.

compared to studies from historical observations (Table 3 and Figure 11). For example, the January–February mean snow depth of 0.33 ± 0.14 m on FYI was higher than the observations during a short test cruise prior to N-ICE2015 in February 2014: here the average snow depth on FYI was 0.20 ± 0.08 on 0.80 m thick sea ice (modal value). It is to be noted that the sea ice in this case was most likely younger and had thus less snow on top.

The April–May mean snow depth for the same region in 2011, reported in local scale studies of Haapala et al. (2013) and Renner et al. (2013) were 0.36 ± 0.26 and 0.32 m, respectively. A 200 m long snow depth profile from 1 April 2003 on 80.427N, 12.817E during Polarstern Cruise ARKTIS-IXI/1 resulted in a mean snow depth of 0.17 ± 0.08 m (Haas, 2018). From the same cruise, average snow and ice thicknesses from ice stations were noted with 0.18 ± 0.14 and 1.96 ± 0.43 m, respectively (Schünemann & Werner, 2005). During a drifting station with Polarstern on Expedition ARKTIS-IX/1 in March 1993 in the same area a 200 m snow and ice thickness profile on 2.56 ± 0.53 m thick MYI indicated an average snow cover of 0.25 ± 0.27 m (Table 3 and Figure 11).

While observations from the recent INTPART Field School 2017 cruise in May to the marginal ice zone north of Svalbard showed a significant number of floes with snow depths larger than 0.4 m (A. Doulgeris et al., personal communication, 2017), alongside FYI floes with much less snow. These observations resemble the conditions during N-ICE2015 and give an indication that the situation of thick snow on thin ice could occur more regularly in this region and might favor an increase in the occurrence of negative freeboard.

In summary, the April to early June mean snow depth of 0.50 ± 0.12 m averaged over all measurements on *Floe 3* (Table 1) was significantly higher than the averaged observations of 0.30 ± 0.14 m from historical observations, including the recent observations from 2017 (Table 3).

Compared to the W99 climatology with values of 0.37 m for snow depth in April in the area north of Svalbard, our observations show thicker snow. It needs to be noted, however, that the use of W99 in the Atlantic Sector of the Arctic should be treated carefully, since observational data are sparse in this region. In fact, only 41 average snow thickness values from the "Sever" Aircraft Landing Observations from the Former Soviet Union from the years 1955 and 1975–1979 (Romanov, 2004) are included in W99 for the area north of Svalbard. W99 describes a general decadal scale decreasing trend in snow depth between 1954 and 1991, but explained by a decrease mainly in May. In addition, a later onset of ice formation (Johnson & Eicken, 2016; Stroeve et al., 2014) and an associated delay in snow accumulation on sea ice, or liquid precipitation instead of snowfall in the autumn, could lead to a general thinning of the snow cover. Nevertheless, interannual and spatial variability of snow thickness is high (Table 3): Forsström et al. (2011) present values in the range of 0.30 ± 0.19 m for Fram Strait in April–May 2005, 2007, and 2008, while Renner et al. (2014) measure 0.32 ± 0.22, 0.47 ± 0.24, and 0.39 ± 0.22 m for the same years, respectively. It is to be noted that the corresponding sea-ice thicknesses are also showing high variability in Forsström et al. (2011) and Renner et al. (2014). Fram Strait is considered a region with high drift speeds and the origin of the sea ice might be different than in the area north of Svalbard (Spreen et al., 2009).

However, exceptional atmospheric circulation events in autumn 2014 and winter 2015 could have caused the observed increased snow depth in 2015 in the study area (Merkouriadi et al., 2017a). Studies suggest that there is evidence, especially for the climate of the Atlantic sector of the Arctic, to shift toward a different regime with a higher storm frequency and more precipitation events, particularly during the winter

Table 3
Snow and Ice Thickness From Historical and Recent Observations in the Area North of Svalbard During April to Early June

Date	Expedition	Mean snow depth (m)	Mean sea-ice thickness (m)	Modal total thickness (m)	Reference
April 1955	"Sever" Aircraft landings	0.16 ± 0.16	0.94 ± 0.42	n/a	Romanov (1996)
April 1974	"Sever" Aircraft landings	0.38 ± 0.12	2.92 ± 0.11	n/a	Romanov (1996)
April 1975	"Sever" Aircraft landings	0.29 ± 0.13	2.28 ± 0.49	n/a	Romanov (1996)
April 1976	"Sever" Aircraft landings	0.46 ± 0.08	2.33 ± 0.10	n/a	Romanov (1996)
April 1977	"Sever" Aircraft landings	0.45 ± 0.16	2.6	n/a	Romanov (1996)
April 1978	"Sever" Aircraft landings	0.16 ± 0.01	2.75 ± 0.35	n/a	Romanov (1996)
April–May 1979	"Sever" Aircraft landings	0.2 ± 0.09	1.93 ± 0.65	n/a	Romanov (1996)
April–May 1954–1991	Climatology	0.37	n/a	n/a	Warren et al. (1999), N-ICE2015 area
March 1993	PS ARKTIS-IX/1	0.25 ± 0.27	2.56 ± 0.43	n/a	Eicken and Meincke (1994)
1 April 2003	PS ARKTIS-IXI/1	0.17 ± 0.08	n/a	n/a	Haas (2018)
April 2003	PS ARKTIS-IXI/1	0.18 ± 0.14	1.96 ± 0.43	n/a	Schünemann and Werner (2005)
18 May to 4 June 2005	Fram Strait	0.32 ± 0.22	2.5 ± 1.1 (total ice and snow)	2.6 ± 1.7	Renner et al. (2014)
10–30 April 2007	Fram Strait	0.47 ± 0.24	2.5 ± 0.9 (total ice and snow)	n/a	Renner et al. (2014)
April–May 2005/2007/2008	Fram Strait	0.30 ± 0.19	1.88 ± 0.83	n/a	Forsström et al. (2011)
16 April to 1 June 2008	Fram Strait	0.39 ± 0.22	3.2 ± 1.1 (total ice and snow)	2.7 ± 1.6	Renner et al. (2014)
April 2009	Polar 5 flight	n/a	n/a	2.4	Haas et al. (2010)
April–May 2011	ICE2011	0.36 ± 0.26	n/a	1.8	Haapala et al. (2013)
April–May 2011	KVS2011/ICE2011	0.32	n/a	1.8	Renner et al. (2013)
February 2014	N-ICE Testcruise	0.20 ± 0.08	n/a	0.80 (FYI)	Unpublished data, NPI
April–June 2015	N-ICE2015	0.53 ± 0.17	1.56 ± 0.51	1.7	This paper, *Floe 3*, EM31/MP(i)
May 2017	INTPART Cruise	0.41 ± 0.23	1.65 ± 0.50	n/a	Unpublished data, NPI

season. This can result in an increased snow thickness (Bintanja & Selten, 2014; Graham et al., 2017a; Merkouriadi et al., 2017a; Park et al., 2015).

Based on ERA-Interim reanalysis data along the back trajectories of the four floes for the months September to March over the period 1979–2015, we see that the winter precipitation has increased. The precipitation experienced by our four floes in winter 2014–2015 lies 50% above the long-term average in our study area (Merkouriadi et al., 2017a). To summarize: in combination with a thinner sea-ice cover (e.g., Hansen et al., 2013; Kwok & Rothrock, 2009) the recently observed amount of snow causes an increase in the snow-ice ratio (this will be even the case if the snow depth is not increasing), which favors negative freeboard and subsequent flooding of the snow pack in the Atlantic sector of the Arctic.

5.3. Thick Snow on Thin Ice Promotes Negative Freeboard

On all four floes widespread negative freeboard along with flooded areas was observed from the drilling records (32–61% of the drill holes show negative freeboard). Also the calculated freeboard indicate widespread negative freeboard, from 5% (*Floe 1*) to 62% (*Floe 2*) of the individual points with snow and ice thickness, when an uncertainty of ±0.06 m is accounted for Figure 6. Of course, part of the negative freeboard values can result from deformation events like ridging, but from the drill hole dataset we have evidence that negative freeboard was common on level ice. Considering the specific densities of snow and ice, the hydrostatic balance is of snow-covered sea ice with a freeboard of 0 cm is given when the ratio of snow depth to ice thickness is approximately 1:3 (Sturm & Massom, 2009). Once this ratio is exceeded—either by accumulating snow on the sea ice or bottom melt of sea ice—and the freeboard becomes negative, lateral flooding or permeation of water through the porous ice with subsequent snow-ice formation can occur. Snow-ice formation is a positive contribution to the sea-ice mass balance and has to be considered in sea-ice models, as snow-ice was found to be widespread during N-ICE2015 (Granskog et al., 2017).

A substantial fraction of areas with negative freeboard can affect regional ice thickness retrievals from satellite altimetry data like CryoSat-2 in two ways: (i) a flooded and saline snow pack will raise the main radar scattering horizon, therefore the sea-ice freeboard might be misinterpreted, which results in erroneously high sea-ice thickness values (Nandan et al., 2017). Further, (ii) areas of negative freeboard might have a disproportionately thick snow cover. For CryoSat-2 ice thickness retrieval algorithms, snow depth values from W99 are widely used, and for FYI dominated regions, it is suggested for calculation of sea-ice thickness to

use only half of the snow depth given in W99 (e.g., Laxon et al., 2013). For the conditions during N-ICE2015, where the observed snow depth in the area north of Svalbard region was 73% higher than the climatological value of W99 for the months April and May, this results in an underestimation of the CryoSat-2 sea-ice thickness product compared to the ground truth data. As an example, with a freeboard of 0.05 m, the calculated sea-ice thickness for $h_s = 0.185$ m (which represents the value of W99/2 which is typically applied for this region), the calculated sea-ice thickness results in 0.87 m for spring conditions (using equation (1)), while with an observed snow thickness of 0.53 m results in an ice thickness of 1.72 m. Another important point to mention in this context is that the presence of thick snow cover might be biased toward higher values in ice thickness (e.g., Kwok, 2014; Ricker et al., 2015). Again, we advise a closer look into the regional characteristics when data are used in a pan-Arctic context, since the observations from the Atlantic sector differ substantially from those of the western Arctic.

6. Conclusion

We have presented a comprehensive data set in which ground-based point measurements from buoys, snow stakes, or drill holes, are complemented by local scale surveys of ice and snow thickness with EM31 and Magnaprobe, and more regional observations with airborne instruments. The N-ICE2015 expedition took place an ice pack composed of SYI, originating from the Laptev Sea in fall 2013 (Itkin et al., 2017), and FYI formed during the drift of the floes with the Transpolar Drift, with some YI formed in leads. From all observations on the individual floes, we find that the average snow depth from January to March 2015 on *Floes 1* and *2* is 0.44 $\pm$ 0.14 m, it shows an increase in April and May 2015 on *Floe 3* to 0.50 $\pm$ 0.12 m and a substantial decrease in June 2015 to 0.31 $\pm$ 0.02 m on *Floe 4*. On the other hand, the average sea-ice thickness remained fairly constant (Figure 3), ranging from 1.2 to 1.3 m (Table 1), until the floes reached the marginal ice zone with strong Atlantic Water influence, where bottom melting occurred (Figure 3).

Irrespective of ice type the modal total snow and ice thickness of 1.6 and 1.7 m inferred from ground-based EM and airborne EM measurements in April, May, and early June 2015, respectively, lie below the values ranging from 1.8 to 2.7 m, reported in historical observations from the same region and time of year. Due to exceptional atmospheric circulation events in autumn 2014 and winter 2015 (Cohen et al., 2017), the observed mean snow depth of 0.53 $\pm$ 0.17 m for April–early June in this region is 73% higher than the average of 0.30 m, ranging from 0.16 to 0.47 m from historical and recent observations (see Table 3).

The thick snow cover affects the sea-ice mass balance on one hand by insulation and slows thermodynamic growth. On the other hand, it leads to negative freeboard of level ice with subsequent flooding and a potential for snow-ice formation. This is exemplified with a positive contribution of snow-ice to the total sea-ice mass balance as found in sea-ice cores collected during N-ICE2015 (Granskog et al., 2017).

Further, snow depth is considered a factor of a high uncertainty in a number of remote sensing and climate modeling applications. Deriving a new pan-Arctic sea-ice snow cover climatology is crucial for further improvement of the satellite based ice thickness products.

The comparison to earlier years suggests that there might be evidence for a regional negative trend in ice thickness and a positive trend for snow depth, while recent observations, i.e., on the INTPART Field School 2017 cruise support that thick snow was not a unique observation. We accept that to some extent we see effects from regional and temporal variability, and to asses this variability, continuous observations of different regions should be performed in the coming years.

The good agreement of measurements on point, local, and regional scales will allow us to take the next step toward upscaling ice classification using satellite images, and make an assessment of the homogeneity of sea-ice cover in the region. This will provide valuable information for sea-ice model parameterizations as well as for sea-ice forecasts, e.g., for navigation and ship route planning in ice.

A repetition of an N-ICE2015-like drift experiment, especially over a longer time period to cover a full cycle of ice growth and ice melt, can be helpful to set our findings on snow and ice thickness in a temporal and spatial context. Prospective expeditions like the planned Multidisciplinary drifting Observatory for the Study of Arctic Climate (MOSAiC) (see science plan at http://www.mosaic-expedition.org/) are highly needed and will give additional value to the previous efforts made in Arctic research.

Acknowledgments
The authors want to thank Andy Mahoney, the two anonymous reviewers, and the editor for their valuable comments which clearly helped to improve the manuscript. We thank the many scientists who collected an incredible amount of observational data. Special thanks to Glen Liston, Jari Haapala, Gunnar Spreen, Jean-Charles Gallet, Nina Maaß, Martine Espeseth, Andrea Gierisch, Annu Oikkonen, Markus Frey, Åse Ervik, Marcel Nicolaus, Chris Polashenski, Anaïs Orsi, and Alexey Shestov. The IMBs and snow buoys were deployed with assistance of Bengt Rotmo, Ottar Skog, Steinar Aksnes, Alf Arne Pettersen, Stephen Hudson, Audun Gjerland, Nina Maaß, Aleksey Pavlov, Gunnar Spreen, Torbjørn Taskjelle, Lana Cohen, and Chris Polashenski. We thank Marius Bratrein for his contribution to the HEM surveys and the design of the hotwire installations. We also thank the crew and scientists on board *R/V Lance*, as well as the helicopter pilots from Airlift AS, and the crew on *KV Svalbard*. Back trajectories of floe drifts were calculated by Gunnar Spreen. The authors thank Glen Liston for his valuable comments on the manuscript and Christian Haas, Donald Perovich, and Stefan Kern for digging in their data archives and helping to find unpublished snow and ice data from previous expeditions. This work has been supported by the Norwegian Polar Institute's Centre for Ice, Climate and Ecosystems (ICE) through the project N-ICE. Additional support and some of the buoys were provided through the projects SMOSice (University Hamburg, ESA, project DFG EXC177), ID Arctic (Norw. Ministries of Foreign Affairs), NFR project STASIS (221961/F20), ICE-ARC (FMI, EU, 7th Framework Programme, grant 603887, paper ICE-ARC-061), and AWI (Helmholtz infrastructure program FRAM). The AWI HEM survey was conducted within the framework of the "Transitions in the Arctic Seasonal Sea Ice Zone" (TRANSSIZ) project. The INTPART Field School 2017 cruise was funded by the INTPART Arctic Field Summer Schools: Norway-Canada-USA collaboration (NFR project 261786/H30). J.K. was supported by the Norwegian Research Council project "CORESAT" (NFR project 222681). N-ICE acknowledges the in-kind contributions provided by other national and international projects and participating institutions, through personnel, equipment, and other support. N-ICE2015 data are available through the Norwegian Polar Data Centre (https://data.npolar.no).

References

Bintanja, R., & Selten, F. M. (2014). Future increases in Arctic precipitation linked to local evaporation and sea-ice retreat. *Nature*, *509*(7501), 479–482. https://doi.org/10.1038/nature13259

Cohen, L., Hudson, S. R., Walden, V. P., & Granskog, M. A. (2017). Meteorological conditions in a thinner Arctic sea ice regime from winter through spring during the Norwegian young sea ICE expedition (N-ICE2015). *Journal of Geophysical Research: Atmospheres*, *122*, 7235–7259. https://doi.org/10.1002/2016JD026034

Comiso, J. C., Parkinson, C. L., Gersten, R., & Stock, L. (2008). Accelerated decline in the Arctic sea ice cover. *Geophysical Research Letters*, *35*, L01703. https://doi.org/10.1029/2007GL031972

Eicken, H., & Meincke, J. (1994). *The expedition ARKTIS-IX/1 of RV "Polarstern" in 1993* (Reports on Polar Research). Bremerhaven, Germany: Alfred Wegener Institute for Polar and Marine Research.

Forsström, S., Gerland, S., & Pedersen, C. A. (2011). Thickness and density of snow-covered sea ice and hydrostatic equilibrium assumption from in situ measurements in Fram Strait, the Barents Sea and the Svalbard coast. *Annals of Glaciology*, *52*(57), 261–270. https://doi.org/10.3189/172756411795931598

Gallet, J.-C., Merkouriadi, I., Liston, G. E., Polashenski, C., Hudson, S. R., Rösel, A., et al. (2017). Spring snow conditions on Arctic sea ice north of Svalbard, during the Norwegian young sea ICE (N-ICE2015) expedition. *Journal of Geophysical Research: Atmospheres*, *122*, 10820–10836. https://doi.org/10.1002/2016JD026035

Gascard, J.-C., Festy, J., le Goff, H., Weber, M., Bruemmer, B., Offermann, M., et al. (2008). Exploring Arctic transpolar drift during dramatic sea ice retreat. *Eos, Transactions American Geophysical Union*, *89*(3), 21. https://doi.org/10.1029/2008EO030001

Geiger, C., Müller, H.-R., Samluk, J. P., Bernstein, E. R., & Richter-Menge, J. (2015). Impact of spatial aliasing on sea-ice thickness measurements. *Annals of Glaciology*, *56*(69), 53–362. https://doi.org/10.3189/2015AoG69A644

Gerland, S., Granskog, M. A., King, J., & Rösel, A. (2017). *N-ICE2015 ice core physics: Temperature, salinity and density [Data set]*. Norway: Norwegian Polar Institute. https://doi.org/10.21334/npolar.2017.c3db82e3

Gerland, S., Renner, A. H. H., Godtliebsen, F., Divine, D., & Løyning, T. B. (2008). Decrease of sea ice thickness at Hopen, Barents Sea, during 1966–2007. *Geophysical Research Letters*, *35*, L06501. https://doi.org/10.1029/2007GL032716

Girard-Ardhuin, F., & Ezraty, R. (2012). Enhanced Arctic sea ice drift estimation merging radiometer and scatterometer data. *IEEE Transactions on Geoscience and Remote Sensing*, *50*(7), 2639–2648.

Graham, R. M., Cohen, L., Petty, A. A., Boisvert, L. N., Rinke, A., Hudson, S. R., et al. (2017b). Increasing frequency and duration of Arctic winter warming events. *Geophysical Research Letters*, *44*, 6974–6983. https://doi.org/10.1002/2017GL073395

Graham, R. M., Rinke, A., Cohen, L., Hudson, S. R., Walden, V. P., Granskog, M. A., et al. (2017a). A comparison of the two Arctic atmospheric winter states observed during N-ICE2015 and SHEBA. *Journal of Geophysical Research: Atmospheres*, *122*, 5716–5737. https://doi.org/10.1002/2016JD025475

Granskog, M., Assmy, P., Gerland, S., Spreen, G., Steen, H., & Smedsrud, L. (2016). Arctic research on thin ice: Consequences of Arctic sea ice loss. *Eos, Transactions American Geophysical Union*, *97*. https://doi.org/10.1029/2016EO044097

Granskog, M. A., Rösel, A., Dodd, P. A., Divine, D., Gerland, S., Martma, T., et al. (2017). Snow contribution to first-year and second-year Arctic sea ice mass balance north of Svalbard. *Journal of Geophysical Research: Oceans*, *122*, 2539–2549. https://doi.org/10.1002/2016JC012398

Haapala, J., Lensu, M., Dumont, M., Renner, A. H., Granskog, M. A., & Gerland, S. (2013). Small-scale horizontal variability of snow, sea-ice thickness and freeboard in the first-year ice region north of Svalbard. *Annals of Glaciology*, *54*(62), 261–266. https://doi.org/10.3189/2013AoG62A157

Haas, C. (2018). *Snow thickness transect north of Svalbard, on 2003-04-01, during POLARSTERN cruise ARK-XIX/1 (PS64)*. Bremerhaven, Germany: Alfred Wegener Institute, Helmholtz Center for Polar and Marine Research, PANGAEA. https://doi.org/10.1594/PANGAEA.885359

Haas, C., Gerland, S., Eicken, H., & Miller, H. (1997). Comparison of sea-ice thickness measurements under summer and winter conditions in the Arctic using a small electromagnetic induction device. *Geophysics*, *62*(3), 749–757. https://doi.org/10.1190/1.1444184

Haas, C., Goff, H. L., Audurain, S., Perovich, D., & Haapala, J. (2011). Comparison of seasonal sea-ice thickness change in the Transpolar Drift observed by local ice mass-balance observations and floe-scale EM surveys. *Annals of Glaciology*, *52*(57), 97–102.

Haas, C., Hendricks, S., Eicken, H., & Herber, A. (2010). Synoptic airborne thickness surveys reveal state of Arctic sea ice cover. *Geophysical Research Letters*, *37*, L09501. https://doi.org/10.1029/2010GL042652

Haas, C., Lobach, J., Hendricks, S., Rabenstein, L., & Pfaffling, A. (2009). Helicopter-borne measurements of sea ice thickness, using a small and lightweight, digital EM system. *Journal of Applied Geophysics*, *67*(3), 234–241. https://doi.org/10.1016/j.jappgeo.2008.05.005

Haas, C., Thomas, D., & Bareiss, J. (2001). Surface properties and processes of perennial Antarctic sea ice in summer. *Journal of Glaciology*, *47*(159), 613–625.

Hansen, E., Ekeberg, O.-C., Gerland, S., Pavlova, O., Spreen, G., & Tschudi, M. (2014). Variability in categories of Arctic sea ice in Fram Strait. *Journal of Geophysical Research: Oceans*, *119*, 7175–7189. https://doi.org/10.1002/2014JC010048

Hansen, E., Gerland, S., Granskog, M. A., Pavlova, O., Renner, A. H. H., Haapala, J., et al. (2013). Thinning of Arctic sea ice observed in Fram Strait: 1990–2011. *Journal of Geophysical Research: Oceans*, *118*, 5202–5221. https://doi.org/10.1002/jgrc.20393

Hudson, S. R., Cohen, L., & Walden, V. P. (2015). *N-ICE2015 surface meteorology v2 [Data set]*. Norway: Norwegian Polar Institute. https://doi.org/10.21334/npolar.2015.056a61d1

Hunke, E. C., Lipscomb, W. H., & Turner, A. K. (2010). Sea-ice models for climate study: Retrospective and new directions. *Journal of Glaciology*, *56*(200), 1162–1172. https://doi.org/10.3189/002214311796406095

Itkin, P., Spreen, G., Cheng, B., Doble, M., Girard-Ardhuin, F., Haapala, J., et al. (2017). Thin ice and storms: Sea ice deformation from buoy arrays deployed during N-ICE2015. *Journal of Geophysical Research: Oceans*, *122*, 4661–4674. https://doi.org/10.1002/2016JC012403

Itkin, P., Spreen, G., Hudson, S. R., Granskog, M. A., Gerland, S., Pavlov, A., et al (2015). *N-ICE2015 buoy data [Data set]*. Norway: Norwegian Polar Institute. https://doi.org/10.21334/npolar.2015.6ed9a8ca

Jackson, K., Wilkinson, J., Maksym, T., Meldrum, D., Beckers, J., Haas, C., et al. (2013). A novel and low-cost sea ice mass balance buoy. *Journal of Atmospheric and Oceanic Technology*, *30*(11), 2676–2688. https://doi.org/10.1175/jtech-d-13-00058.1

Johnson, M., & Eicken, H. (2016). Estimating Arctic sea-ice freeze-up and break-up from the satellite record: A comparison of different approaches in the Chukchi and Beaufort Seas. *Elementa: Science of the Anthropocene*, *4*, 124. https://doi.org/10.12952/journal.elementa.000124

Kaleschke, L., Tian-Kunze, X., Maas, N., Ricker, R., Hendricks, S., & Drusch, M. (2015). Improved retrieval of sea ice thickness from SMOS and CryoSat-2. In *IEEE International Geoscience and Remote Sensing Symposium (IGARSS)*. IEEE. https://doi.org/10.1109/igarss.2015.7327014

King, J., Gerland, S., Spreen, G., & Bratrein, M. (2016). *N-ICE2015 sea-ice thickness measurements from helicopter-borne electromagnetic induction sounding [Data set]*. Norway: Norwegian Polar Institute. https://doi.org/10.21334/npolar.2016.aa3a5232

King, J., Spreen, G., Gerland, S., Haas, C., Hendricks, S., Kaleschke, L., et al. (2017). Sea-ice thickness from field measurements in the northwestern Barents Sea. *Journal of Geophysical Research: Oceans*, *122*, 1497–1512. https://doi.org/10.1002/2016JC012199

Kovacs, A., & Morey, R. M. (1991). Sounding sea ice thickness using a portable electromagnetic induction instrument. *Geophysics*, *56*(12), 1992–1998. https://doi.org/10.1190/1.1443011

Kurtz, N. T., Farrell, S. L., Studinger, M., Galin, N., Harbeck, J. P., Lindsay, R., et al. (2013). Sea ice thickness, freeboard, and snow depth products from Operation IceBridge airborne data. *The Cryosphere*, *7*(4), 1035–1056. https://doi.org/10.5194/tc-7-1035-2013

Kwok, R. (2014). Simulated effects of a snow layer on retrieval of CryoSat-2 sea ice freeboard. *Geophysical Research Letters*, *41*, 5014–5020. https://doi.org/10.1002/2014GL060993

Kwok, R., & Cunningham, G. F. (2015). Variability of Arctic sea ice thickness and volume from CryoSat-2. *Philosophical Transactions of the Royal Society*, *373*, 20140157. https://doi.org/10.1098/rsta.2014.0157

Kwok, R., & Rothrock, D. A. (2009). Decline in Arctic sea ice thickness from submarine and ICESat records: 1958–2008. *Geophysical Research Letters*, *36*, L15501. https://doi.org/10.1029/2009GL039035

Laxon, S. W., Giles, K. A., Ridout, A. L., Wingham, D. J., Willatt, R., Cullen, R., et al. (2013). CryoSat-2 estimates of Arctic sea ice thickness and volume. *Geophysical Research Letters*, *40*, 732–737. https://doi.org/10.1002/grl.50193

Lindsay, R., & Schweiger, A. (2015). Arctic sea ice thickness loss determined using subsurface, aircraft, and satellite observations. *The Cryosphere*, *9*(1), 269–283. https://doi.org/10.5194/tc-9-269-2015

Maaß, N., Kaleschke, L., Tian-Kunze, X., & Drusch, M. (2013). Snow thickness retrieval over thick Arctic sea ice using SMOS satellite data. *The Cryosphere*, *7*(6), 1971–1989. https://doi.org/10.5194/tc-7-1971-2013

Mahoney, A. R., Eicken, H., Fukamachi, Y., Ohshima, K. I., Simizu, D., Kambhamettu, C., et al. (2015). Taking a look at both sides of the ice: Comparison of ice thickness and drift speed as observed from moored, airborne and shore-based instruments near Barrow, Alaska. *Annals of Glaciology*, *56*(69), 363–372. https://doi.org/10.3189/2015AoG69A565

Mahoney, A., Gearheard, S., Oshima, T., & Qillaq, T. (2009). Sea ice thickness measurements from a community-based observing network. *Bulletin of the American Meteorological Society*, *90*(3), 370–377. https://doi.org/10.1175/2008BAMS2696.1

Marshall, H. P., Koh, G., Sturm, M., Johnson, J., Demuth, M., Landry, C., et al. (2006). Spatial variability of the snowpack: Experiences with measurements at a wide range of length scales with several different high precision instruments. In J.A. Gleason (Ed.), *Proceedings of. ISSW 2006* (pp. 359–364), Telluride, CO: International Snow Science Workshop Proceedings - Montana State University Library. Retrieved from http://arc.lib.montana.edu/snow-science/item.php?id=947

Maslanik, J., Stroeve, J., Fowler, C., & Emery, W. (2011). Distribution and trends in Arctic sea ice age through spring 2011. *Geophysical Research Letters*, *38*, L13502. https://doi.org/10.1029/2011GL047735

Meier, W. N., Hovelsrud, G. K., van Oort, B. E. H., Key, J. R., Kovacs, K. M., Michel, C., et al. (2014). Arctic sea ice in transformation: A review of recent observed changes and impacts on biology and human activity. *Reviews of Geophysics*, *52*, 185–217. https://doi.org/10.1002/2013RG000431

Merkouriadi, I., Gallet, J.-C., Liston, G., Polashenski, C., Itkin, P., King, J., et al. (2017b). *N-ICE2015 snow pit data [Data set]*. Norway: Norwegian Polar Institute. https://doi.org/10.21334/npolar.2017.d2be5f05

Merkouriadi, I., Gallet, J.-C., Liston, G. E., Polashenski, C., Rösel, A., & Gerland, S. (2017a). Winter snow conditions over the Arctic Ocean north of Svalbard during the Norwegian young sea ICE (N-ICE2015) expedition. *Journal of Geophysical Research: Atmospheres*, *122*, 10837–10854. https://doi.org/10.1002/2017JD026753

Meyer, A., Fer, I., Sundfjord, A., & Peterson, A. K. (2017a). Mixing rates and vertical heat fluxes north of Svalbard from Arctic winter to spring. *Journal of Geophysical Research: Oceans*, *122*, 4569–4586. https://doi.org/10.1002/2016JC012441

Meyer, A., Sundfjord, A., Fer, I., Provost, C., Robineau, N. V., Koenig, Z., et al. (2017b). Winter to summer hydrographic and current observations in the Arctic Ocean north of Svalbard. *Journal of Geophysical Research: Oceans*, *122*, 6218–6237. https://doi.org/10.1002/2016JC012391

Nandan, V., Geldsetzer, T., Yackel, J., Mahmud, M., Scharien, R., Howell, S., et al. (2017). Effect of snow salinity on CryoSat-2 Arctic first-year sea ice freeboard measurements. *Geophysical Research Letters*, *44*, 10419–10426. https://doi.org/10.1002/2017GL074506

Newman, T., Farrell, S. L., Richter-Menge, J., Connor, L. N., Kurtz, N. T., Elder, B. C., et al. (2014). Assessment of radar-derived snow depth over Arctic sea ice. *Journal of Geophysical Research: Oceans*, *119*, 8578–8602. https://doi.org/10.1002/2014JC010284

Park, D.-S. R., Lee, S., & Feldstein, S. B. (2015). Attribution of the recent winter sea ice decline over the Atlantic Sector of the Arctic Ocean. *Journal of Climate*, *28*(10), 4027–4033. https://doi.org/10.1175/JCLI-D-15-0042.1

Peeken, I. (2015). *Station list and links to master tracks in different resolutions of POLARSTERN cruise PS92 (ARK-XXIX/1 TRANSSIZ)*. Bremerhaven-Longyearbyen: Alfred Wegener Institute, Helmholtz Center for Polar and Marine Research, Bremerhaven, PANGAEA. https://doi.org/10.1594/PANGAEA.848841

Perovich, D., Richter-Menge, J., Polashenski, C., Elder, B., Arbetter, T., & Brennick, O. (2014). Sea ice mass balance observations from the North Pole Environmental Observatory. *Geophysical Research Letters*, *41*, 2019–2025. https://doi.org/10.1002/2014GL059356

Perovich, D. K. (2003). Thin and thinner: Sea ice mass balance measurements during SHEBA. *Journal of Geophysical Research: Oceans*, *108*(C3), 8050. https://doi.org/10.1029/2001JC001079

Peterson, A. K., Fer, I., McPhee, M. G., & Randelhoff, A. (2017). Turbulent heat and momentum fluxes in the upper ocean under Arctic sea ice. *Journal of Geophysical Research: Oceans*, *122*, 1439–1456. https://doi.org/10.1002/2016JC012283

Pfaffhuber, A. A., Hendricks, S., & Kvistedal, Y. A. (2012). Progressing from 1D to 2D and 3D near-surface airborne electromagnetic mapping with a multisensor, airborne sea-ice explorer. *Geophysics*, *77*(4), WB109–WB117. https://doi.org/10.1190/geo2011-0375.1

Polashenski, C., Perovich, D., Richter-Menge, J., & Elder, B. (2011). Seasonal ice mass-balance buoys: Adapting tools to the changing Arctic. *Annals of Glaciology*, *52*(57), 9.

Provost, C., Sennéchael, N., Miguet, J., Itkin, P., Rösel, A., Koenig, Z., et al. (2017). Observations of flooding and snow-ice formation in a thinner Arctic sea ice regime during the N-ICE2015 campaign: Influence of basal ice melt and storms. *Journal of Geophysical Research: Oceans*, *122*, 7115–7134. https://doi.org/10.1002/2016JC012011

Radionov, V. F., Bryazgin, N. N., & Alexandrov, E. I. (1997). *The snow cover of the Arctic Basin* (Tech. Rep. Tech. Rep. APL-UW-TR 9701). Seattle, WA: Applied Physics Laboratory, University of Washington.

Renner, A. H. H., Gerland, S., Haas, C., Spreen, G., Beckers, J. F., Hansen, E., et al. (2014). Evidence of Arctic sea ice thinning from direct observations. *Geophysical Research Letters*, *41*, 5029–5036. https://doi.org/10.1002/2014GL060369

Renner, A. H. H., Hendricks, S., Gerland, S., Beckers, J., Haas, C., & Krumpen, T. (2013). Large-scale ice thickness distribution of first-year sea ice in spring and summer north of Svalbard. *Annals of Glaciology*, *54*(62), 13–18. https://doi.org/10.3189/2013AoG62A146

Richter-Menge, J. A., & Farrell, S. L. (2013). Arctic sea ice conditions in spring 2009–2013 prior to melt. *Geophysical Research Letters*, *40*, 5888–5893. https://doi.org/10.1002/2013GL058011

Ricker, R., Hendricks, S., Kaleschke, L., Tian-Kunze, X., King, J., & Haas, C. (2017). A weekly Arctic sea-ice thickness data record from merged CryoSat-2 and SMOS satellite data. *The Cryosphere*, *11*(4), 1607–1623. https://doi.org/10.5194/tc-11-1607-2017

Ricker, R., Hendricks, S., Perovich, D. K., Helm, V., & Gerdes, R. (2015). Impact of snow accumulation on CryoSat-2 range retrievals over Arctic sea ice: An observational approach with buoy data. *Geophysical Research Letters*, *42*, 4447–4455. https://doi.org/10.1002/2015GL064081

Rinke, A., Maturilli, M., Graham, R. M., Matthes, H., Handorf, D., Cohen, L., et al. (2017). Extreme cyclone events in the Arctic: Wintertime variability and trends. *Environmental Research Letters*, *12*(9), 094006. https://doi.org/10.1088/1748-9326/aa7def

Romanov, I. P. (1996). *Atlas of ice and snow of the Arctic Basin and Siberian Shelf Seas* (vol. 211, 250 charts). Paramus, NJ: Backbone Publishing.

Romanov, I. P. (2004). *Morphometric characteristics of ice and snow in the Arctic Basin: Aircraft landing observations from the former Soviet Union, 1928–1989, Version 1*. Boulder, CO: National Snow and Ice Data Center. https://doi.org/10.7265/N5B8562T

Rösel, A., Bratrein, M., King, J. A., Itkin, P., Divine, D., Ervik, A., et al. (2016b). *N-ICE2015 ice thickness from hot wires [Data set]*. Norway: Norwegian Polar Institute. https://doi.org/10.21334/npolar.2016.263a317f

Rösel, A., Divine, D., King, J. A., Nicolaus, M., Spreen, G., Itkin, P., et al. (2016c). *N-ICE2015 total (snow and ice) thickness data from EM31 [Data set]*. Norway: Norwegian Polar Institute. https://doi.org/10.21334/npolar.2016.70352512

Rösel, A., Itkin, P., Divine, D., King, J. A., Nicolaus, M., Polashenski, et al. (2016a). *N-ICE2015 snow thickness from snow stakes [Data set]*. Norway: Norwegian Polar Institute. https://doi.org/10.21334/npolar.2016.3099ea95

Rösel, A., & King, J. (2017). *N-ICE2015 ice thickness, snow thickness, and freeboard from thickness drillings [Data set]*. Norway: Norwegian Polar Institute. https://doi.org/10.21334/npolar.2017.25f70db1

Rösel, A., Polashenski, C. M., Liston, G. E., King, J. A., Nicolaus, M., Gallet, J.-C., et al. (2016d). *N-ICE2015 snow depth data with Magna Probe [Data set]*. Norway: Norwegian Polar Institute. https://doi.org/10.21334/npolar.2016.3d72756d

Schünemann, H., & Werner, I. (2005). Ice station data during POLARSTERN expeditions ARK-XVIII/2 and ARK-XIX/1 to Fram Strait, the western Barents Sea and north of Svalbard, https://doi.org/10.1594/PANGAEA.855170, supplement to: Schünemann, H.,; Werner, I (2004). Seasonal variations in distribution patterns of sympagic meiofauna in Arctic pack ice. *Marine Biology*, *146*(6), 1091–1102. https://doi.org/10.1007/s00227-004-1511-7.

Spreen, G., Kern, S., Stammer, D., & Hansen, E. (2009). Fram Strait sea ice volume export estimated between 2003 and 2008 from satellite data. *Geophysical Research Letters*, *36*, L19502. https://doi.org/10.1029/2009GL039591

Stroeve, J., Holland, M. M., Meier, W., Scambos, T., & Serreze, M. (2007). Arctic sea ice decline: Faster than forecast. *Geophysical Research Letters*, *34*, L09501. https://doi.org/10.1029/2007GL029703

Stroeve, J. C., Markus, T., Boisvert, L., Miller, J., & Barrett, A. (2014). Changes in Arctic melt season and implications for sea ice loss. *Geophysical Research Letters*, *41*, 1216–1225. https://doi.org/10.1002/2013GL058951

Sturm, M. (2002). Winter snow cover on the sea ice of the Arctic Ocean at the Surface Heat Budget of the Arctic Ocean (SHEBA): Temporal evolution and spatial variability. *Journal of Geophysical Research*, *107*(C10), 8047. https://doi.org/10.1029/2000JC000400

Sturm, M., & Holmgren, J. (1999). *Self-recording snow depth probe*. U.S. patent 5,864,059. Google Patents. Retrieved from https://www.google.com/patents/US5864059

Sturm, M., & Massom, R. A. (2009). Snow and sea ice. In D. N. Thomas & G. S. Dieckmann (Eds.), *Sea ice* (2nd ed.). Oxford, UK: Wiley-Blackwell. https://doi.org/10.1002/9781444317145.ch5

Wang, C., Granskog, M. A., Hudson, S. R., Gerland, S., Pavlov, A. K., Perovich, D. K., et al. (2016). Atmospheric conditions in the central Arctic Ocean through the melt seasons of 2012 and 2013: Impact on surface conditions and solar energy deposition into the ice-ocean system. *Journal of Geophysical Research: Atmospheres*, *121*, 1043–1058. https://doi.org/10.1002/2015JD023712

Warren, S. G., Rigor, I. G., Untersteiner, N., Radionov, V. F., Bryazgin, N. N., Aleksandrov, Y. I., et al. (1999). Snow depth on Arctic sea ice. *Journal of Climate*, *12*(6), 1814–1829. https://doi.org/10.1175/1520-0442

Webster, M. A., Rigor, I. G., Nghiem, S. V., Kurtz, N. T., Farrell, S. L., Perovich, D. K., et al. (2014). Interdecadal changes in snow depth on Arctic sea ice. *Journal of Geophysical Research: Oceans*, *119*, 5395–5406. https://doi.org/10.1002/2014JC009985

Weeks, W., & Ackley, S. (1986). *The growth, structure and properties of sea ice, vol. The geophysics of sea ice*. New York, NY: Plenum Press.

Woods, C., & Caballero, R. (2016). The role of moist intrusions in winter Arctic warming and sea ice decline. *Journal of Climate*, *29*(12), 4473–4485. https://doi.org/10.1175/JCLI-D-15-0773.1